Global Biogeochemical Cycles

RESEARCH ARTICLE
10.1029/2019GB006513

Mineral Nutrients Sourced in Deep Regolith Sustain Long-Term Nutrition of Mountainous Temperate Forest Ecosystems

D. Uhlig[1,2], W. Amelung[3], and F. von Blanckenburg[1,4]

[1]GFZ German Research Centre for Geosciences, Earth Surface Geochemistry, Potsdam, Germany, [2]Now at Forschungszentrum Jülich GmbH, Institute of Bio- and Geosciences (IBG-3) Agrosphere, Jülich, Germany, [3]Institute of Crop Science and Resource Conservation (INRES), Soil Science and Soil Ecology, University of Bonn, Bonn, Germany, [4]Also at Institute of Geological Sciences, Freie Universität Berlin, Berlin, Germany

Key Points:
- Combined ^{87}Sr(radiogenic)/^{86}Sr and ^{10}Be(cosmogenic)/^{9}Be isotope ratios were applied as proxies for mineral nutrient uptake depth
- These systems suggest mineral nutrient uptake by *Picea abies* and *Fagus sylvatica* of 2 to >10 m depth
- Potentially biologically available calcium phosphate is not available at a depth shallower than 3 m
- Loss of mineral nutrients from the nutrient-rich forest floor is balanced by mineral nutrient uptake from the deep saprolite

Correspondence to:
D. Uhlig,
d.uhlig@fz-juelich.de

Citation:
Uhlig, D., Amelung, W., & von Blanckenburg, F. (2020). Mineral nutrients sourced in deep regolith sustain long-term nutrition of mountainous temperate forest ecosystems. *Global Biogeochemical Cycles*, *34*, e2019GB006513. https://doi.org/10.1029/2019GB006513

Received 23 DEC 2019
Accepted 13 AUG 2020
Accepted article online 19 AUG 2020

Abstract Primary productivity of forest ecosystems depends on the availability of plant-essential mineral nutrients. Because nutrient demand of trees often exceeds nutrient supply from rock, tree nutrition is sustained by efficient reutilization of organic-bound nutrients. These nutrients are continuously returned from trees to the forest floor in litterfall. However, over millennia nutrient limitation may develop in landscapes from which nutrients are permanently lost by drainage and erosion. Such a deficit is prevented if advection of unweathered bedrock toward the surface as driven by erosion continuously supplies fresh nutrients. Yet the mechanisms and the depth range over which this deep nutrient resource is accessed are poorly known. We show that in two montane temperate forest ecosystems in the Black Forest and Bavarian Forest the geogenic source of nutrients was found within a depth zone of several meters. This deep zone contains a large pool of biologically available nutrients. We applied isotope ratios as proxies for nutrient uptake depth, and we tracked the regolith depth at which the isotope ratios of $^{87}Sr/^{86}Sr$ and ^{10}Be(meteoric)/^{9}Be match the respective values in plant tissue. We mapped the depth distribution of the biologically available calcium-bound form of the most plant-essential mineral nutrient phosphorus and found that the depth of phosphorus availability is as deep or even deeper as the range defined by the isotope ratios. We conclude that nutrient supply from a regolith depth of several meters is critical for forest ecosystem function in landscapes of moderate hillslopes and rainfall that are affected by permanent nutrient loss.

1. Introduction

A key regulator of primary productivity in forest ecosystems is the availability of nutrients (Fernández-Martínez et al., 2014). Because uptake fluxes of plant-essential mineral nutrients such as phosphorus (P), potassium (K), calcium (Ca), and magnesium (Mg) into forest trees often exceed nutrient supply fluxes from mineral weathering (e.g., Cleveland et al., 2013; Newman, 1995; Uhlig & von Blanckenburg, 2019a), forest trees have evolved strategies to prevent nutrient limitation. For example, nutrients that are continuously returned from trees through litterfall to the forest floor can be efficiently reutilized or, in other words, are recycled from plant litter and soil biomass (called here "organic" sources) (Jobbagy & Jackson, 2000; Lang et al., 2016; Turner et al., 2013; Vitousek & Farrington, 1997). Indeed, the magnitude of this organic mineral nutrient turnover exceeds geochemical release fluxes from primary minerals by a factor of between 5 and 100 (e.g., Riotte et al., 2014; Schuessler et al., 2018; Uhlig et al., 2017; Wilcke et al., 2017). This cycle has been called the "organic nutrient pathway" (Uhlig & von Blanckenburg, 2019a).

Even though recycling of nutrients minimizes their loss from the forest ecosystem (e.g., Jobbágy & Jackson, 2001, 2004), a minor fraction is nevertheless continuously lost by solute export, erosion, or both. For example, for the most plant-growth limiting mineral nutrient P, the dissolved (Bol et al., 2016) or colloidal (Gottselig et al., 2020; Missong et al., 2016) loss caused by dissolution of minerals or by plant litter leaching (Cleveland et al., 2006) typically amounts to 1–60 mg m^{-2} $year^{-1}$ and can be as much as 240 mg m^{-2} $year^{-1}$ (Bol et al., 2016). In addition, due to the tight binding of P to organic matter and soil minerals, 90% of total P loss may actually occur via particulate export (Tiessen, 2008), where fine particulate export amounts to losses of up to 800 mg P m^{-2} $year^{-1}$ (Meyer & Likens, 1979). Finally, P loss may also occur through erosion of plant litter (e.g., Heartsill Scalley et al., 2012; Scatena & Lugo, 1995). Such dissolved or

particulate losses are not restricted to the mineral nutrient P. Estimates of the loss of other mineral nutrients from temperate forest ecosystems were recently provided by Uhlig et al. (2017) and Uhlig and von Blanckenburg (2019a). Importantly, however, while mineral nutrient losses from the forest floor are too small to affect tree nutrition within annual timescales, the continuous deficit from nutrient loss means that the mineral nutrient pool in forest floor material should diminish significantly after ~10 to 100 years, depending on pool sizes (e.g., Uhlig & von Blanckenburg, 2019a) and in the absence of additional input. Since this is equal to or less than the lifetime of a tree, nutrient limitation would in this scenario inevitably inhibit plant-growth.

To balance this continuous loss of mineral nutrients over millennial timescales and sustain primary productivity, external supply from atmospheric wet deposition and dust deposition have been suggested (Chadwick et al., 1999). However, in mountainous settings, typical atmospheric deposition rates of, for example, P (Aciego et al., 2017) are mostly much smaller than P losses (Uhlig et al., 2017). Similarly, studies from Likens et al. (1977) in the Hubbard Brook Experimental Forest and from Johnson (1989) in the Walker Branch Watershed showed a net deficit of the plant-essential mineral nutrients K, Ca, and Mg when atmospheric deposition is considered as the only input fraction. The existence of a negative nutrient balance suggests that atmospheric inputs are lower than outbound fluxes from organic forest floor materials or from weathering. If atmospheric inputs fail to replenish mineral nutrients, one means suggested to prevent a decline phase in forest ecosystem development are catastrophic disturbances such as mass wasting events like landslides (e.g., Stallard, 1995; Wardle et al., 2004), which expose fresh, nutrient-rich material that is less weathered than the soil removed. These events are limited to tectonically active landscapes of high-relief, and thus such episodic mass wasting is not a viable replenishment mechanism in the majority of Earth's mountainous forest ecosystems.

Porder et al. (2007) suggested that the development of nutrient limitation is countered over millennial timescales by the advection of nutrients locked in primary minerals across the weathering front, driven by erosion. The process causing this transfer is chemical weathering that converts bedrock into regolith (Graham et al., 2010)—where regolith is defined here to comprise mobile soil and immobile saprolite (chemically weathered bedrock that is *in situ* and has retained its original fabric; Becker, 1895). This mechanism pertains to landscapes that are slowly but permanently eroding such that the surface material depleted in mineral nutrients is replaced by fresh material from below. For example, half of the terrestrial surface slopes by more than 5° (Larsen et al., 2014), and simply by the forces of gravity, experiences permanent loss of mineral nutrients through erosion or drainage. In such eroding settings nutrient availability in the weathering zone varies vertically (Porder et al., 2007) rather than temporally (Walker & Syers, 1976). A corollary of this idea is that the source from which nutrients are supplied is shifted into the weathering front. This front is located at sometimes considerable depth and certainly below the depth of soils that are commonly considered to encompass all sources of plant nutrition.

Another mechanism suggested to supply nutrients from depth is nutrient uplift by biota. Jobbágy and Jackson (2004) provided evidence for nutrient uplift through an increase in concentration of soil exchangeable K, Na, and Mg at topsoil. Bullen and Chadwick (2016) demonstrated by means of Ca, Sr, and Ba stable isotopes that there is an upward flux of nutrients from depth via plant uptake that is subsequently returned to the topsoil as litterfall. Moreover, increasing evidence currently emerges that the deeper subsoil is an important source for water and nutrients to plants (Dawson et al., 2020). For example deep fine roots do indeed take up both water and nutrients from up to 12 m depth (Germon et al., 2020). Thus, nutrient uplift by plants is the mechanism we explore in this study.

To do so we build on previous findings by Uhlig and von Blanckenburg (2019a) which show for the two mountainous, temperate forest ecosystems explored further in this study that the deep saprolite hosts a reservoir of biologically available mineral nutrients and that this nutrient reservoir is in turn continuously replenished by rock weathering over thousands of years. This replacement flux was called the “geogenic nutrient pathway” and is instrumental in satisfying the “geogenic nutrient supply” (De Oliveira Garcia et al., 2018) required in many forest ecosystems. Yet the Uhlig and von Blanckenburg (2019a) study lacked direct evidence that nutrients are indeed taken up from the deep saprolite. Here we fingerprint the mean depth from which mineral nutrients are sourced to compensate loss of organic-bound nutrients and to ultimately sustain forest growth. To this end we explored nutrient sources in cores that were drilled up to 30 m deep through

regolith into unweathered bedrock. We used radiogenic strontium isotope ratios ($^{87}Sr/^{86}Sr$) to bracket the depth of mineral nutrient uptake. For the same purpose we established a second and independent isotope system, namely, the cosmogenic meteoric beryllium isotope ratio ($^{10}Be(meteoric)/^{9}Be$) as a novel proxy for the depth of mineral nutrient sources. Finally, we determined the depth distribution of the different chemical forms in which the most plant-essential mineral nutrient P is bound. A geochemical background dataset measured on these drill cores was provided by Uhlig and von Blanckenburg (2019a, 2019b).

2. Conceptual Framework

2.1. Using Element and Isotope Ratios as Fingerprints of Nutrient Uptake Depth

The overarching rationale of using element or isotope ratios as conservative proxy of nutrient uptake depth is that a given element or isotope ratio varies with regolith depth. The depth-dependent ratios of a biologically available regolith compartment are compared with those found in living plant tissue, to estimate the average nutrient uptake depth, above and below which nutrient uptake may take place (e.g., Coble et al., 2015; McCulley et al., 2004). This depth has been identified in previous studies by means of element ratios, isotope labeling experiments, or radiogenic isotope ratios, each approach having strengths and weaknesses.

Element ratios such as Ca/Sr or Ge/Si are relatively simple to measure, but as it turns out, are unsuitable because they often shift during plant uptake and during translocation within plants. For example, Sr is discriminated as compared to Ca during the translocation from the belowground to the aboveground plant organs (e.g., Blum et al., 2008, 2012; Drouet & Herbauts, 2008; Pett-Ridge, Derry, & Barrows, 2009; Poszwa et al., 2000), and Ge is discriminated against Si during plant uptake (e.g., Blecker et al., 2007; Delvigne et al., 2009; Derry et al., 2005). Isotope labeling is an alternative approach, in which a specific soil horizon is labeled with artificially enriched isotopes of a plant-essential element (e.g., Chapin & Van Cleve, 2000) such as ^{15}N (e.g., Ackermann et al., 2015), ^{44}Ca or ^{26}Mg (e.g., van der Heijden et al., 2013). For this application, the isotope ratio of the label applied is suitably anomalous that the effect of any isotope fractionation during plant uptake is negligible. The reliability of this procedure for assessing the depth of nutrient uptake is questionable, however, because the addition of an isotope tracer inevitably entails fertilization. Moreover, isotope labeling experiments are cost-intensive and the injection of the isotope tracer into a specific soil horizon can be challenging, as the label may move through preferential flow pathways or react with unlabeled nutrient pools.

A third class of depth indicators makes use of naturally occurring radiogenic isotopes. A prerequisite is that the radiogenic isotope ratio varies with depth. For the radiogenic strontium isotope ratio ($^{87}Sr/^{86}Sr$), for example, a depth gradient develops if parent bedrock comprises multiple Sr-containing primary minerals of different mineral solubility and with distinct $^{87}Sr/^{86}Sr$ ratios. Measured $^{87}Sr/^{86}Sr$ ratios are thought to serve as a proxy for the depth of Ca uptake, due to the similar chemical properties of Sr and Ca, and have successfully been used to fingerprint the Ca source in boreal forest ecosystems (e.g., Åberg et al., 1990; Bailey et al., 1996; Bélanger et al., 2012; Blum et al., 2002; Bullen & Bailey, 2005; Miller et al., 1993), temperate forest ecosystems (e.g., Bedel et al., 2016; Drouet et al., 2005, 2005; Kennedy et al., 2002; Meek et al., 2016; Schmitt et al., 2017), and tropical forest ecosystems (e.g., Pett-Ridge, Derry, & Kurtz, 2009; Pett-Ridge, Derry, & Barrows, 2009). $^{87}Sr/^{86}Sr$ ratios have also been used to trace the depth of nutrient uptake more generally in arid and semiarid ecosystems (e.g., Coble et al., 2015; Jackson et al., 2002; McCulley et al., 2004), boreal forest ecosystems (e.g., Poszwa et al., 2004), temperate forest ecosystems (e.g., Berger et al., 2006; Poszwa et al., 2003), and tropical rainforests (e.g., Poszwa et al., 2002, 2009). We utilize this established method for our study sites and thus discuss it in more detail in section 2.2.

Taking advantage of early geomorphic studies on meteoritic ^{10}Be (Bacon et al., 2012; Brown et al., 1992; McKean et al., 1993), we introduce a new system here: the $^{10}Be(meteoric)/^{9}Be$ isotope ratio. It uses the rare radioactive cosmogenic fallout nuclide $^{10}Be(meteoric)$ in combination with the stable isotope ^{9}Be that is released in trace amounts during rock weathering. This isotope system was originally developed to quantify total denudation rates from soil and bedload sediment (von Blanckenburg et al., 2012) and has been successfully applied to forest ecosystems in very small and very large watersheds (e.g., Dannhaus et al., 2018; Wittmann et al., 2015, respectively). Here we leverage the strong depth dependency of the $^{10}Be(meteoric)/^{9}Be$ ratio in regolith (detailed later in section 2.3) to devise a new method to trace nutrient uptake depth.

2.2. Radiogenic Strontium ($^{87}Sr/^{86}Sr$) as Tracer for Nutrient Sources

Natural Sr consists of four stable isotopes: ^{84}Sr, ^{86}Sr, ^{87}Sr, and ^{88}Sr. Among them ^{87}Sr is a so-called radiogenic isotope, as ^{87}Sr is the product of the radioactive β^- decay of ^{87}Rb with a half-life of ~4.88×10^{10} years (Holden, 1990). In contrast to stable isotope systems, isotope fractionation is not measured with radiogenic Sr, because any natural or instrumental isotope shifts are corrected for during mass spectrometry by the normalization of the measured $^{87}Sr/^{86}Sr$ ratio to the known natural ratio of $^{88}Sr/^{86}Sr = 8.375209$ (e.g., Faure & Mensing, 2005).

Strontium is a trace element in the continental crust and due to its high solubility during chemical weathering Sr is strongly partitioned into water. Although Sr is a non-nutritive element, plant roots nevertheless take up Sr along with Ca via non-selective cation channels, due to their identical valency and similar electron configurations. Even though the chemical properties of the macronutrients K, Mg, and P differ from those of Sr and Ca we regard it as likely that the uptake depth of K, Mg, and P can also be traced by radiogenic Sr provided that during weathering these elements are released from primary minerals into the dissolved pore water fraction at similar depth. Depth profiles of elemental loss in our cores have shown that this is a reasonable assumption (Uhlig & von Blanckenburg, 2019a). To use $^{87}Sr/^{86}Sr$ as nutrient source tracer we compared the $^{87}Sr/^{86}Sr$ ratio of living wood and foliage with the "biologically available" fraction of Sr in the drill-cores. Here, this biologically available fraction is operationally defined and is thought to represent the most loosely held mineral nutrients in the soil. These comprise the water-soluble and the easily exchangeable fraction (e.g., Bacon & Davidson, 2008; Filgueiras et al., 2002) that are assumed to be in equilibrium with soil pore water and are steadily replenished by primary mineral dissolution. Moreover, the exchangeable fraction forms weak electrostatic bonds with the negative surfaces of phyllosilicates and clay minerals or organic matter. Using the operationally defined biologically available fraction instead of directly analyzing Sr from soil water offers considerable advantages: The biologically available fraction can be extracted with high depth resolution from a sampled regolith depth profile, whereas lysimeters sample soil water only at few depth intervals, and their installation likely disturbs the integrity of soil and generates preferential flow pathways leading to perturbed and unrepresentative infiltration of water. We assume that the biologically available fraction of Sr in the forest floor and organic-rich topsoil is mainly sourced from decomposed organic matter and in the mineral soil and saprolite primarily stems from *in situ* dissolution of primary minerals.

2.3. Cosmogenic Meteoric Beryllium ($^{10}Be(meteoric)/^{9}Be$) as Tracer for Nutrient Sources

Beryllium has one stable isotope, namely, ^{9}Be. As cosmic radiation enters the Earth's atmosphere spallation reactions take place and produce so-called cosmogenic nuclides, such as meteoric ^{10}Be. Due to its geologically short half-life of 1.4 Myr, meteoric ^{10}Be is not an original constituent of rocks. Instead, meteoric ^{10}Be is scavenged by rainwater after production and infiltrates into soil. Conversely, ^{9}Be occurs in trace amounts in rock (von Blanckenburg et al., 2012), specifically in the minerals plagioclase, mica, and K-feldspar (e.g., Navrátil, 2000; Skřivan et al., 2000), and is released by rock weathering into soil solution. Both meteoric-derived ^{10}Be and mineral-derived ^{9}Be mix in soil water from which they are coprecipitated into amorphous and poorly crystalline oxides (am-ox). However, ^{10}Be and ^{9}Be may also be as passively taken up by plants as Mg by transporters of the MGT family (Maathuis, 2009) to substitute for Mg (Kabata-Pendias, 2011). Thus, the $^{10}Be(meteoric)/^{9}Be$ isotope ratio of amorphous and poorly crystalline oxides represents that of the operationally defined biologically available fraction of regolith fluids. Because of the reactive nature of hydrolyzed Be (e.g., $BeOH^+$ or $Be(OH)_2$) and the distinct sources of these two isotopes, the $^{10}Be(meteoric)/^{9}Be$ ratio follows a bulge-shaped depth profile and below the bulge decreases strongly with regolith depth (Maher & von Blanckenburg, 2016). Isotope fractionation effects can be neglected for Be because the analytical uncertainty of typically 5% exceeds any isotope fractionation effect expected for $^{10}Be/^{9}Be$ that from the similarity of the neighboring $^{7}Li/^{6}Li$ and $^{11}B/^{10}B$ systems is typically 10^1 per mil (Faure & Mensing, 2005). Thus, the depth distribution of the $^{10}Be(meteoric)/^{9}Be$ ratio represents a promising tracer to fingerprint the depth of nutrient uptake, for which it is used in this study for the very first time.

2.4. Phosphorus

Phosphorus fulfills diverse life-sustaining functions in all living organisms. Among the essential mineral nutrients, P commonly limits plant growth (Augusto et al., 2017; Du et al., 2020; Vance et al., 2003). Yet P

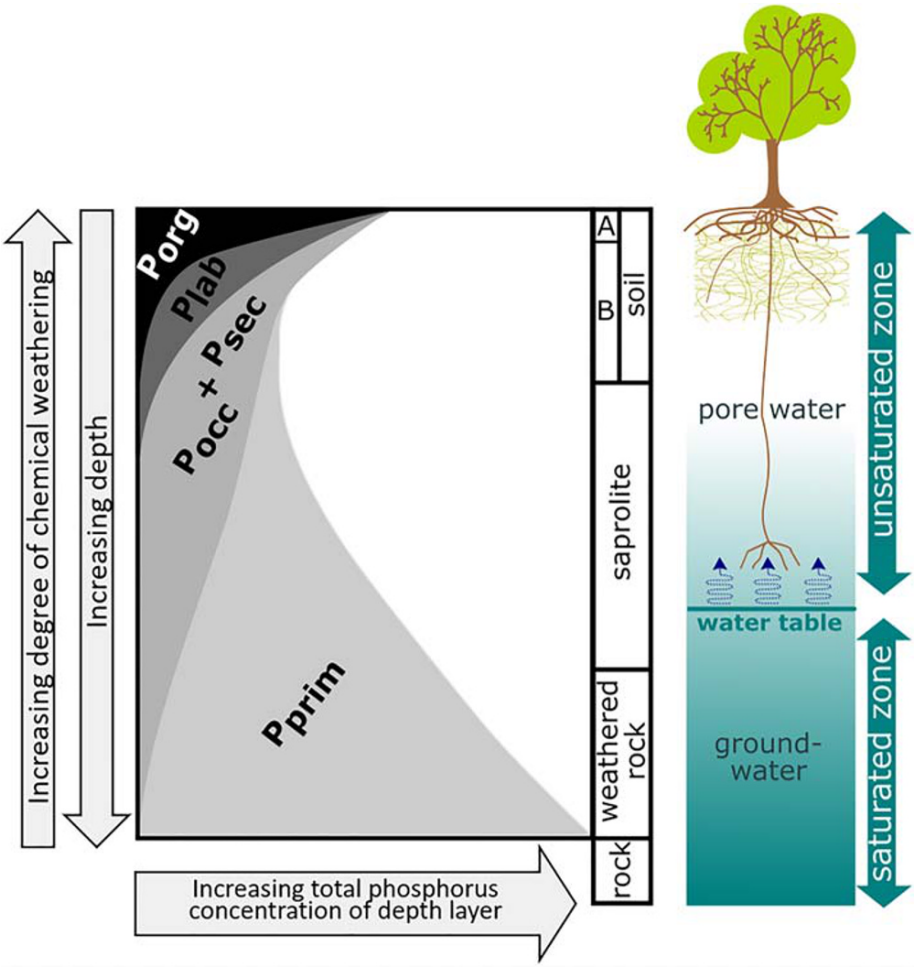

Figure 1. Hypothesized depth distribution of extractable phosphorus (P) with depth and nutrient uptake pathways. The left-hand part of this figure is redrawn from Walker and Syers (1976) by rotating the Walker and Syers figure by 90° to illustrate P fractions with depth. In permanently eroding settings the P forms depend on uplift and erosion of soil particles in the weathering zone (Porder et al., 2007). Phosphorus uptake pathways shown here are: deep rooting, dimorphic root systems, capillary rise (blue arrows), symbiotic relationship between roots, and mycorrhizal fungi (yellow network). Phosphorus fractions shown here are organic-bound P (P_{org}) corresponding to the P Hedley fractions resin-P_o + NaOH-P_o + $NaHCO_3$-P_o (Table 1), labile P (P_{lab}) corresponding to the P Hedley fraction resin-P_i, occluded and secondary P (P_{occ} + P_{sec}) corresponding to the P Hedley fractions $NaHCO_3$-P_i + NaOH-P_i + HCl_{conc}-P_{total} + Residual P_{total} (Table 1), primary mineral-bound P (P_{prim}) corresponding to the P Hedley fraction HCl_{dil}-P_i. A, B: Soil horizons.

is present in only trace amounts in host rock (e.g., Porder & Ramachandran, 2013), and over millennia, the inventory of mineral-bound P in soil decreases by mineral dissolution. Water flow and ensuing soil chemical reactions also reduce the availability of P to trees by the transformation of biologically available P (e.g., dissolved P and P adsorbed onto soil minerals) into P forms that are not readily biologically available (e.g., P occluded within sesquioxides) (e.g., Helfenstein et al., 2018; Walker & Syers, 1976). An established method to compartmentalize soil P is the Hedley sequential phosphorus fractionation (Hedley et al., 1982). Operationally defined P forms examined in this study are resin-extractable P, 0.5 M $NaHCO_3$-extractable P, 0.1 M NaOH-extractable P, 1 M HCl-extractable P, and concentrated HCl-extractable P. These P forms are assumed to mirror organic bound P, biologically available non-occluded P, potentially biologically available Ca-bound P, and biologically unavailable occluded P. According to the classical Walker and Syers (1976) model the inventory of P forms depends on soil age. In sloping landscapes, in contrast to the models from Wardle et al. (2004) and Walker and Syers (1976), gradients in chemical weathering develop vertically rather than with time (Porder et al., 2007, Figure 1). Thus, we assume a

depth gradient in the P forms that allows conclusions on the availability and thus possible uptake depth of potentially biologically available P to be drawn.

3. Study Sites

Nutrient uptake depths were determined in two southern German upland forest ecosystems, which are monitored by the International Co-operative Program on assessment and monitoring of air pollution effects on forests (ICP Forests) and are study sites of the DFG priority program SPP 1685 "Ecosystem Nutrition – Forest Strategies for limited Phosphorus Resources." Neither site was glaciated during the last glacial maximum (LGM). The Black Forest (Conventwald, site CON, 48°1.20222′N, 7°57.93996′E) is characterized by a moderate hillslope of 17°, mean annual precipitation (MAP) of 1,400 mm, mean annual temperature (MAT) of 7.9°C, and by a Hyperdystric skeletic folic Cambisol (Baxter, 2007). The Bavarian Forest (Mitterfels, site MIT, 48°58.54860′N, 12°52.49388′E) is characterized by a gentle hillslope of 10°, MAP of 1,300 mm, MAT of 4.5°C and by a Hyperdystric chromic folic Cambisol (Baxter, 2007). European beech (*Fagus sylvatica*) and Norway spruce (*Picea abies*) of about 130 years age (Lang et al., 2017) dominate the tree species at CON and MIT. Both study sites are underlain by paragneiss, while the Cambisols developed on periglacial slope deposits formed during the LGM, as is common in the northern hemisphere (Kleber & Terhorst, 2013). The presence of periglacial slope deposits of typically less than 3 m thickness (Kleber & Terhorst, 2013) implies that no substantial mass wasting events such as landslides occurred at our study sites since the LGM. Total denudation rates from *in situ* cosmogenic nuclides, which integrate physical erosion and chemical weathering losses over several thousands of years, are 125 t km^{-2} $year^{-1}$ at CON and 57 t km^{-2} $year^{-1}$ at MIT (Uhlig & von Blanckenburg, 2019a). Because the mineralogical composition of the paragneiss is shifted toward more soluble minerals at CON than at MIT the chemical weathering rate is with 71 t km^{-2} $year^{-1}$ much higher at CON than at MIT (8 t km^{-2} $year^{-1}$). Thus, the regolith at CON is substantially more depleted in mineral nutrients than at MIT.

4. Methods

4.1. Sampling

Forest floor samples originate from soil pits sampled by Lang et al. (2017) near the drill sites at each study site. Regolith was sampled at depth increments of 20 cm from a 3 m deep trench. Regolith beyond 3 m depth and unweathered parent bedrock were sampled from 20 m (CON) and 30 m (MIT) deep drill cores. Living wood, leaves, and needles were sampled from representative mature trees of the prevailing species *Fagus sylvatica* and *Picea abies*. A more detailed description of the sampling is provided in Uhlig and von Blanckenburg (2019a).

We note that the combination of drilling, chemical extraction of elements from soil and saprolite, and the application of two isotope systems, from which the Be system represents an entirely new tracer for the nutrient uptake depth, represents considerable methodological development. The labor-intensive nature of these initial tests precluded the employment of these systems to multiple sample replicates.

4.2. Analytical Methods

Sample preparation, radiogenic Sr isotope measurements, ^{9}Be concentration measurements, sample purification prior to ^{10}Be analysis, and soil pH analysis were performed at the Helmholtz Laboratory for the Geochemistry of the Earth Surface (HELGES) at GFZ-Potsdam (von Blanckenburg et al., 2016). Hedley sequential phosphorus fractionation was performed at the University of Bonn, Institute of Crop Science and Resource Conservation INRES. Cosmogenic ^{10}Be analyses were performed at the University of Cologne – Centre for Accelerator Mass Spectrometry.

4.2.1. Extracting the Biologically Available Fraction of Strontium

The biologically available fraction of Sr comprises the water-soluble fraction and the exchangeable fraction. Each extraction was performed on a suspension of 2 g of bulk soil (dried, sieved to <2 mm) in 14 ml of reactant, where deionized water (Milli-Q, 18 MΩ) was used for the water-soluble extraction and 1 M NH_4OAc at neutral pH for the exchangeable fraction. The suspension was first dispersed in an ultrasonic bath for 1 hr and then gently shaken on a hotdog roller at 7 rpm for 24 hr (water-soluble extraction) and 2 hr (exchangeable extraction), respectively. After shaking the suspension was centrifuged at 4,200 rpm for 30 min, and the

supernatant was pipetted off into a syringe and filtered through a 0.2 μm acetate filter. The entire sequential extraction method was repeated once for each sample. Both individual supernatants were combined, treated as one sample with concentrated acid mixtures (HF, HCl, and HNO_3), and redissolved prior to radiogenic Sr analyses.

4.2.2. Analyzing the Radiogenic Sr ($^{87}Sr/^{86}Sr$) Ratios

Prior to radiogenic Sr analysis rock and regolith samples and reference materials were dissolved by a silicate digestion method using ultrapure concentrated acid mixtures (HCl, HNO_3, HF, and H_2O_2) in PFA vials. Vegetation samples and the plant reference material SRM 1515 (apple leaves, NIST) were digested using a microwave method (MLS start) with ultrapure acid mixtures (H_2O_2, HNO_3, HCl, and HF) in PFA vials. After sample digestion Sr was separated from matrix elements using inverted disposable pipettes packed with 200 μl TrisKem SR-B50-S (50–100 μm) resin (Sr-Spec). Matrix elements were removed by elution with 5.5 ml 7.5 M HNO_3 and Sr was eluted with 2 ml deionized water (Milli-Q water, 18.2 MΩ). To destroy any organic crown-ether released from the Sr-Spec resin, the Sr fraction was dried, redissolved and treated in closed PFA vials for more than 12 hr in a concentrated acid mixture (H_2O_2 and HNO_3) at 85°C and then in concentrated HNO_3 at 170°C. The purity of the Sr fraction was monitored by ICP-OES (Varian 700E) analysis. Impurities were negligible except in the case of Ba, which was kept below a Ba/Sr ratio of less than 5, below which doping tests with SRM 987 demonstrated no resultant analytical bias. $^{87}Sr/^{86}Sr$ was measured on a multi collector inductively coupled plasma mass spectrometer (MC-ICP-MS, Thermo Neptune) using an APEX-Q (ESI) as sample introduction system, a low mass resolution slit and 40 ng g^{-1} pure Sr solutions in 0.3 M HNO_3. The blank to sample ratio on ^{88}Sr was less than 0.4%. Simultaneously to the signals of ^{84}Sr (L2), ^{86}Sr (central Faraday Cup), ^{87}Sr (H1), and ^{88}Sr (H2) we monitored the signals of ^{82}Kr (L4), ^{83}Kr (L3), and ^{85}Rb (L1) to correct for Kr and Rb interferences on the masses 84 and 87 with the Kr and Rb isotope ratios measured prior to the sequence run. The measured $^{87}Sr/^{86}Sr$ ratio was normalized to the $^{88}Sr/^{86}Sr$ ratio of 8.375209 using an exponential law to correct for natural and instrumental isotope fractionation. Repeat analyses of SRM 987 both processed through chemistry and without chemistry was used to determine the long-term accuracy of the method. Averages and two standard deviations are SRM 987 = 0.71029 ± 0.00001 (N = 240, without chemistry) and SRM 987 = 0.71026 ± 0.00011 (N = 32, including chemistry) and are identical to published values for SRM 987 = 0.71029 ± 0.00033 (N = 247; Jochum et al., 2005) measured with MC-ICP-MS.

4.2.3. Extraction and Analyses of Amorphous and Poorly Crystalline Oxides

Amorphous and poorly crystalline oxides (am-ox) were separated following the procedure described in Wittmann et al. (2012). The method is based on Fe isotope studies where the biologically available fraction of Fe, which includes the pools of water-extractable, exchangeable Fe, organically bound or adsorbed Fe, and poorly crystalline Fe oxides, were sequentially extracted (Guelke et al., 2010). Although not analyzed, we separated the adsorbed exchangeable fraction prior to the am-ox extraction step to allow optimal comparison of the chemical composition of leachates from the Be extraction and Sr extraction procedure. The Be concentration of the exchangeable fraction of Be is typically negligible when compared to the am-ox fraction (Wittmann et al., 2012). We added 10 ml 1 M $MgCl_2$ to 0.5 g bulk soil (dried and sieved to <63 μm), shook the suspension for more than 12 hr, centrifuged for 20 min at 4,200 rpm and pipetted off the supernatant. We then washed the sample three times using 10 ml deionized water at pH 9 (Milli-Q, 18.2 MΩ, pH adjusted with ammonia) and discarded the wash solutions. Finally, the amorphous and poorly crystalline oxides were separated by adding 10 ml 0.5 M HCl and by mild shaking for 24 hr. The supernatant was pipetted off as the exchangeable fraction and treated with concentrated acid mixtures (HF, HCl, and HNO_3). Next, two aliquots were taken for separate analyses of ^{9}Be and ^{10}Be.

The ^{9}Be concentration of amorphous oxides was measured with ICP-OES in 0.3 M HNO_3 and matrix matched calibration standards with a relative uncertainty of 5% based on accuracy of repeat analyses of the international reference materials GA (granite, CNRS) and RGM-1 (rhyolite, USGS).

4.2.4. Analyzing the $^{10}Be(meteoric)/^{9}Be$ Ratio

^{9}Be concentrations were analyzed as described in Uhlig, Goldberg, et al. (2020). In summary, ^{9}Be of plant matter was measured on an iCAP-Q with fast pump system (ESI Fast DX, 1 ml loop) with uncertainties better than 16% relative based on repeat digestion and analyses of SRM 1515 (apple leaves, NIST). Prior to ^{9}Be analyses of plant matter the sample matrix was reduced by several orders of magnitudes by cation-exchange chromatography using inverted disposable pipettes packed with 3 ml AG50W-X12 resin (200–400 mesh).

Table 1
Sequential Fractionation Scheme and Resulting P Fractions and Their Properties (Slightly Modified From Barej et al., 2014)

Fraction	Extraction procedure[a]	Fraction properties[b]
Resin-P_i	Anion exchange resin, 16 hr	Labile P_i, biologically most available P form
Resin-P_o		Water-soluble organic P_o, usually present in only trace amounts
$NaHCO_3$-P_i	0.5 M $NaHCO_3$ pH 8.5, 16 hr	Labile P_i, likely to be biologically available, associated with Fe and Al oxides
$NaHCO_3$-P_o		Easily mineralizable P_o
NaOH-P_i	0.1 M NaOH, 16 hr	Moderately labile P_i, associated with secondary Fe and Al oxides
NaOH-P_o		Stable P_o, resulting from long-term transformation of P forms
HCl_{dil}-P_i	1 M HCl, 16 hr	Moderately stable P_i, Ca-bound P, associated with primary minerals (e.g., apatite), considered as potentially biologically available
HCl_{dil}-P_o		Rarely present, Ca-precipitated P_o and P_o associated with sesquioxides (e.g., Al_2O_3 and Fe_2O_3) dissolving in HCl
HCl_{conc}-P_{tot}	HCl_{conc}, 80°C 10 min	Very stable P, covers recalcitrant P occluded in sesquioxides (e.g., Al_2O_3 and Fe_2O_3)
Residual P_{tot}	*Aqua regia* digestion	Highly refractory and occluded P forms
Summed fractions		
Org-P	Sum of P_o: $NaHCO_3$-P_o, NaOH-P_o, resin-P_o	
HCl_{dil}-P_{tot}	Sum of HCl_{dil}-P_i and HCl_{dil}-P_o	

Note. P_i denotes inorganic P forms (measured by the molybdenum blue method). P_o denotes organic-bound P (measured from P_{total} minus P_i).
[a]According to Tiessen and Moir (1993) and Hedley et al. (1982). [b]Based on Tiessen and Moir (1993) and Cross and Schlesinger (1995).

After cation-exchange chromatography, the ^{9}Be aliquot was sufficiently purified to avoid matrix effects during iCAP-Q analysis.

^{10}Be(meteoric) aliquots were spiked depending on the natural ^{9}Be concentration with 400 to 550 μg of our in-house ^{9}Be "phenakite" carrier (^{9}Be: 372.5 μg g^{-1}). The matrix elements were separated from the spiked ^{10}Be aliquot using anion and cation chromatography methods and alkaline precipitation described in detail in von Blanckenburg et al. (1996, 2004). ^{10}Be(meteoric)/^{9}Be analyses were performed by accelerator mass spectrometry (AMS) at University Cologne. Procedure blanks were subtracted from the samples.

4.2.5. Determining the P Forms by the Hedley Fractionation Method

To identify P forms that are plant available, sieved, and ground aliquots from the cores were extracted sequentially in duplicate according to a modified Hedley procedure (Tiessen & Moir, 1993). The Hedley procedure entails a stepwise chemical extraction of P forms from 0.5 g soil at a 1:60 soil:solution ratio (w/v). Resin-P was extracted in the presence of an anion-exchange resin and deionized water; $NaHCO_3$-P in 0.5 M $NaHCO_3$, NaOH-P in 0.1 M NaOH and HCl_{dil} in 1 M HCl, each at an extraction time of 16 hr in an overhead shaker, followed by centrifugation and filtration through ashless quantitative paper filters (Albet LabScience, Dassel, Germany). Subsequently, the HCl_{conc}-P_{total} fraction was extracted with hot concentrated HCl (80°C, 20 min). For the final extraction of "residual P," we used *aqua regia* following Lauer et al. (2013). For each fraction, we determined inorganic-bound P (P_i) by the molybdenum-blue method (Murphy & Riley, 1962) and total P by ICP-OES (Ultima 2, HORIBA Jobin Yvon, Longjumeau, France); organic-bound P (P_o) was calculated as the difference of total P and P_i. As the HCl_{conc} and residual P fractions of weathered bedrock are usually devoid of significant amounts of organic-bound P (Lauer et al., 2013; and references in Cross & Schlesinger, 1995), these extracts were analyzed by ICP-OES only. A detailed description of the sequential extraction scheme of P and the fraction properties is provided in Table 1. We note that the total P concentrations derived from XRF analyses of bulk regolith differ from the sum of P fractions derived from Hedley fractionation by on average ~10%. The disparities may arise from the low sensitivity of XRF for P, or the possibility of non-quantitative Hedley extraction steps (e.g., Lauer et al., 2013 and unpublished data). Nevertheless, we used both methods for the assessment of weathering depth.

4.2.6. Analyzing the Soil pH

The pH of soil and saprolite was assessed on a suspension of 1 g oven dried (60°C, 24 hr) bulk soil (<2 mm fraction) and 5 ml 0.01 M $CaCl_2$ with a WTW pH meter. Prior to soil pH measurements the suspension was dispersed for 10 min in an ultrasonic bath and shaken for 20 min on a Stuart rocker and roller mixer. For quality control, the Merck pH 4 buffer solution and the international reference material IRMM-443-7 (Cambisol, BCR/IRMM representing the same soil type as those at our study sites) were analyzed after

Table 2
Fluxes of Atmospheric Deposition (Wet and Dust) and Chemical Weathering

	K		Ca		Mg		P		Reference
External atmospheric dust deposition flux estimates (mg m^{-2} $year^{-1}$)									
Dep^{X}_{dust} (min) dust-derived	37		59		21		1.6		See section 4.2.7.
Dep^{X}_{dust} (max) dust-derived	110		180		63		4.8		See section 4.2.7.
Dep^{X}_{dust} (min) UCC-derived	50		54		24		1.3		See section 4.2.7.
Dep^{X}_{dust} (max) UCC-derived	150		170		73		3.9		See section 4.2.7.
Dep^{X}_{dust} (min)	**37**		**54**		**21**		**1.3**		
Dep^{X}_{dust} (max)	**150**		**180**		**73**		**4.8**		
Compiled atmospheric dust deposition fluxes (mg m^{-2} $year^{-1}$)									
	Min	Max	Min	Max	Min	Max	Min	Max	
Atmospheric dust	11	30	82	171	6	9	—	—	Morselli et al. (2008)
Atmospheric dust	23	226	36	361	12	123	1	11	Lawrence and Neff (2009)
Atmospheric dust	—	—	—	—	—	—	5	10	Mahowald et al. (2008)
Atmospheric dust	—	—	—	—	—	—	0.7	11	Aciego et al. (2017)
Atmospheric dust	—	—	230		—	—	—	—	De Angelis and Gaudichet (1991)
Atmospheric wet deposition fluxes (mg m^{-2} $year^{-1}$)									
Dep^{X}_{wet} (CON)[a]	160		380		53		7.1		Uhlig and von Blanckenburg (2019a)
uncertainty	*57*		*79*		*11*		*5.5*		
Dep^{X}_{wet} (MIT)[b]	340		380		73		46		Uhlig and von Blanckenburg (2019a)
uncertainty	*220*		*79*		*27*		*35*		
Chemical weathering fluxes (mg m^{-2} $year^{-1}$)									
$W^{X}_{regolith}$ (CON)	1,000		5,500		2,000		84		Uhlig and von Blanckenburg (2019a)
uncertainty	*160*		*480*		*210*		*10*		
$W^{X}_{regolith}$ (MIT)	240		980		400		65		Uhlig and von Blanckenburg (2019a)
uncertainty	*130*		*150*		*33*		*12*		

Note. Dep^{X}_{dust}: External atmospheric dust deposition flux of element X. Dep^{X}_{wet}: Atmospheric wet deposition flux of element X. $W^{X}_{regolith}$: Chemical weathering flux of element X (release flux of X from minerals minus the flux of incorporation of X into secondary minerals and regolith oxides). Italic values denote uncertainties.
[a]Data provided by the Forstliche Versuchsanstalt Baden-Wuerttemberg (FVA). [b]Data provided by the Bayerische Landesanstalt für Wald und Forstwirtschaft (LWF).

every tenth sample. The soil pH analyses were stable and accurate, and the reproducibility was better than ±1.5%. Soil pH data are presented in Table S1.

4.2.7. Estimating Atmospheric Dust Deposition Fluxes

Atmospheric wet deposition fluxes (Dep^{X}_{wet}, Table 2)—defined here as comprising dissolved atmospheric constituents deposited by rain, snow or fog above the tree canopy—were routinely monitored at CON by the Forstliche Versuchsanstalt Baden-Wuerttemberg (FVA) and at MIT by the Bayerische Landesanstalt für Wald und Forstwirtschaft (LWF). External atmospheric dust deposition fluxes (Dep^{X}_{dust}, Table 2)—defined here as comprising mineral dust particles sourced from external locations such as deserts—were not monitored at either study site. We thus estimated external atmospheric dust deposition fluxes of element X by multiplying published total dust deposition rates with element concentrations typical of dust. Minima and maxima of total dust deposition rates (Table S2) were taken from global dust deposition maps provided by Jickells et al. (2005) and Zender et al. (2003), both of which rely on modeled data. Concentration data of atmospheric dust were compiled from Avila et al. (1998), Castillo et al. (2008), Goudie and Middleton (2001), Hladil et al. (2008), Lawrence and Neff (2009), and Vanderstraeten et al. (2008). To provide a representative estimate of Dep^{X}_{dust} we used this comparison set of concentrations along with the composition of the upper continental crust (UCC, data from Taylor & McLennan, 1995). We multiplied the minima and maxima of total dust deposition rates with these concentrations. Notably, the weighted mean concentrations of atmospheric dust and UCC differ by only 25%. We preferred this use of compiled data over using measured data from a single location (such as from the nearby Strengbach catchment or the Alps) because the considerable spatiotemporal variability of eolian dust input means no one site is necessarily representative of our study sites' dust deposition flux. However, to assess whether the magnitude of our estimates of Dep^{X}_{dust} is reasonable, we also tabulated measured atmospheric dust deposition fluxes from European sites in the Alps and Northern Italy and globally distributed sites and found that these are in the same range (Table 2).

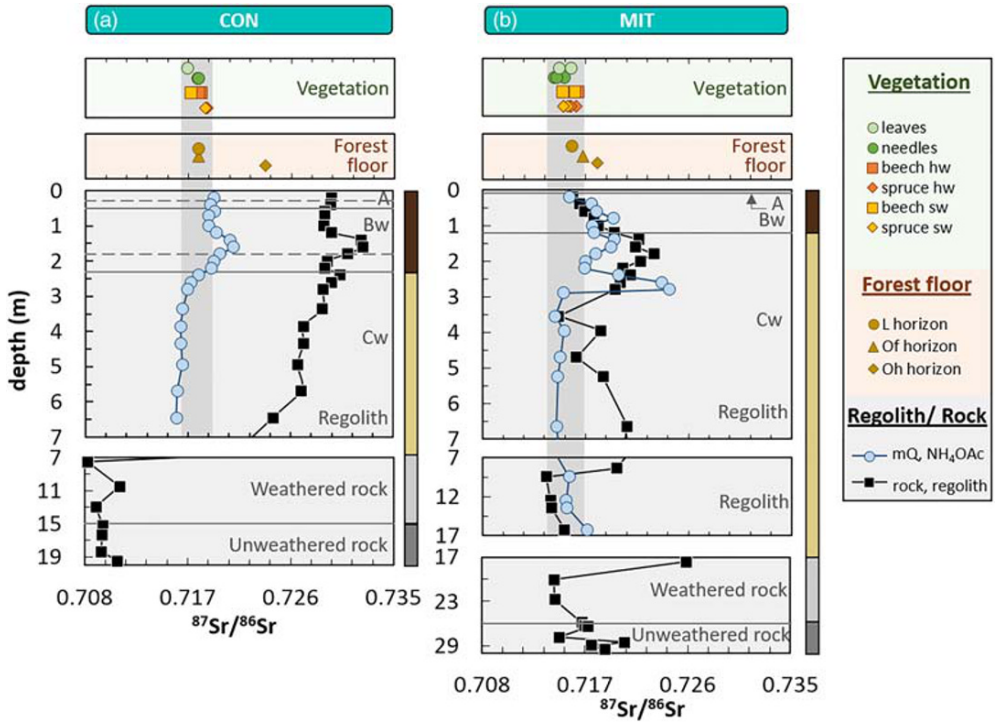

Figure 2. Depth distribution of $^{87}Sr/^{86}Sr$ in plants, regolith, rock and the biologically available fraction comprising the water-soluble (deionized water, pH 5) and 1 M NH_4OAc extractable fraction at CON (panel a) and MIT (panel b). hw: heartwood, sw: sapwood. L: litter layer, Of: organic fermented layer, Oh: organic humic layer. A, Bw, Cw: soil horizons. Horizontal stippled lines subdivide soil horizons (A into Ah and Ah+Bw, B into Bw1 and Bw2). Gray vertical bar: range of vegetation $^{87}S/^{86}Sr$. Colored bars at the right side of panels (a) and (b) assign data to soil (brown), saprolite (beige), weathered rock (light gray), unweathered rock (dark gray). Note that *y*-axis spacing changes with depth for ease of display.

5. Results

5.1. Radiogenic Strontium Isotope Ratio

The radiogenic strontium isotope ratio ($^{87}Sr/^{86}Sr$) of bulk regolith shifts at CON from low ratios of 0.7094 to 0.7109 in bedrock to high ratios of 0.7245 to 0.7327 in regolith (Figure 2, Table S3). At MIT, in contrast, $^{87}Sr/^{86}Sr$ of bulk regolith ranges from 0.7148 to 0.7205 which is similar to bulk parent rock with $^{87}Sr/^{86}Sr$ from 0.7136 to 0.7230 (Figure 2, Table S3). The difference in these patterns can be explained with the higher degree of chemical weathering at CON than at MIT. At CON plagioclase, which is typically relatively high in the concentration of Sr but shows low $^{87}Sr/^{86}Sr$ ratios (e.g., Hewawasam et al., 2013; Pett-Ridge, Derry, & Kurtz, 2009), is almost entirely lost from the regolith, whereas biotite, which is typically relatively low in Sr concentration but has a high $^{87}Sr/^{86}Sr$ ratio (e.g., Hewawasam et al., 2013; Pett-Ridge, Derry, & Kurtz, 2009), remains in the regolith (Uhlig & von Blanckenburg, 2019a). The paragneiss at MIT is dominated by a more Na-rich plagioclase which has lower solubility upon weathering and is hence retained in the profile (Uhlig & von Blanckenburg, 2019a) resulting in less weathering impact on the $^{87}Sr/^{86}Sr$ of bulk regolith.

The biologically available fraction of Sr at CON has much lower $^{87}Sr/^{86}Sr$ (0.7160 to 0.7212) than bulk regolith, and its depth distribution mirrors the $^{87}Sr/^{86}Sr$ depth distribution of bulk regolith (Figure 2, Table S3). At MIT, in contrast, the $^{87}Sr/^{86}Sr$ depth distribution of the biologically available fraction ranges from 0.7109 to 0.7244, which is similar to that of bulk regolith, yet it does not show a systematic correlation with the patterns seen in bulk regolith (Figure 2, Table S3). The difference between the profiles can also be explained by the difference in weatherability: At CON, Sr with low $^{87}Sr/^{86}Sr$ primarily released from Ca-rich plagioclase is found in the biologically available fraction. The systematic gradients in the $^{87}Sr/^{86}Sr$ ratio of the NH_4OAc-extractable fraction and its mirroring of the $^{87}Sr/^{86}Sr$ of bulk regolith within the uppermost 3 m indicate

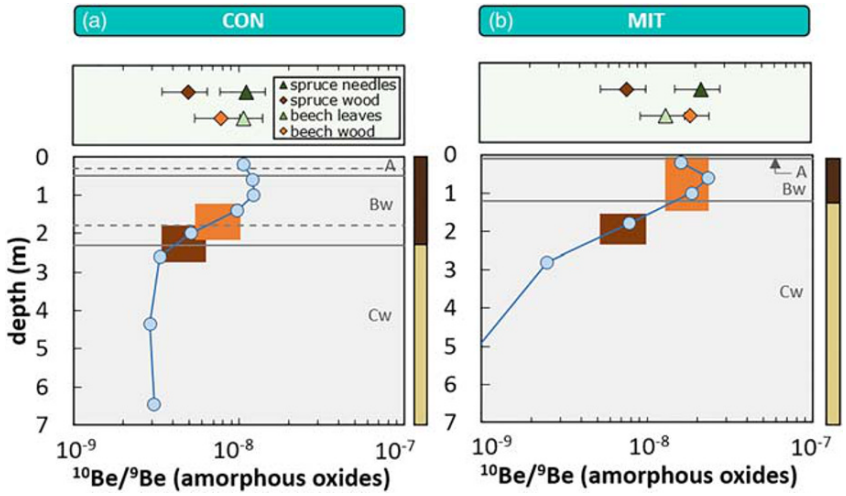

Figure 3. Fingerprinting nutrient uptake depth by comparing ^{10}Be(meteoric)/^{9}Be in vegetation with the depth profile of ^{10}Be(meteoric)/^{9}Be in amorphous oxides (representing the potentially biologically fraction of Be) at CON (panel a) and MIT (panel b). Vertical bars: range of ^{10}Be(meteoric)/^{9}Be of stem wood from *Fagus sylvatica* (light brown) and *Picea abies* (dark brown). A, Bw, Cw: soil horizons. Horizontal stippled lines subdivide soil horizons (A into Ah and Ah+Bw, B into Bw1 and Bw2). Colored bars at the right side of panels (a) and (b) assign data to soil (brown) and saprolite (beige).

that Sr solubilization from upper layers and its translocation to deeper layers is not a predominant process. Rather its gradients reflect variations in the release and isotope composition of Sr from remaining primary minerals. This assumption is supported by the concentrations of all major elements in the biologically available fraction at both study sites (Uhlig & von Blanckenburg, 2019a). Most of these are higher at >3 m depth than above, suggesting release at depth rather than transport from above.

The Sr isotope composition of plant material reveals two important results. The first is that ^{87}Sr/^{86}Sr ratios of leaf foliage (CON: 0.7170–0.7179, MIT: 0.7142–0.7158) and wood (CON: 0.7173–0.7186, MIT: 0.7150–0.7163) are roughly identical to the ratios in the L and Of horizon (CON: 0.7179, MIT: 0.7158–0.7168) in the forest floor (Figure 2, Table S4) at both sites. This isotope matching confirms the dominance of an "organic nutrient cycle" (Uhlig & von Blanckenburg, 2019a) because Sr and other organic-bound mineral nutrients are efficiently reutilized from the forest floor. This recycling process is most efficient for P and K at both sites (Uhlig & von Blanckenburg, 2019a). The second important result is relevant to the identification of the initial geogenic Sr source. ^{87}Sr/^{86}Sr of living plant matter is identical to ^{87}Sr/^{86}Sr of the biologically available fraction over the deeper sections of the weathering zone, namely, from 2 to 7 m depth at CON and from 3 to 17 m depth at MIT (Figure 2, Table S3). This finding indicates that the Sr found in the forest floor and organic soil layers is initially sourced from these deep regolith layers demonstrating a slow but permanent "geogenic nutrient pathway" (Uhlig & von Blanckenburg, 2019a). Such a nutrient uptake depth is deeper than previously found in temperate and boreal forest ecosystems (e.g., Berger et al., 2006; Poszwa et al., 2003, 2004), but as deep as in arid to semiarid grass- and shrublands (Coble et al., 2015; Jackson et al., 2002; McCulley et al., 2004).

5.2. Cosmogenic Meteoric Beryllium Isotope Ratio

At both sites, the depth distribution of the cosmogenic meteoric beryllium isotope ratio (^{10}Be(meteoric)/^{9}Be) in amorphous and poorly crystalline oxides (am-ox) follows a bulge shape. Maximum values of 12×10^{-9} at CON and 23×10^{-9} at MIT are found in ^{10}Be(meteoric)/^{9}Be of the Bw soil horizon, and minimum values of 2.9×10^{-9} at CON and 0.02×10^{-9} at MIT are found in the saprolite (Figure 3, Table S5). ^{10}Be(meteoric)/^{9}Be ratios in leaf foliage are about 11×10^{-9} at CON and to 13×10^{-9} (*Fagus sylvatica*) and 21×10^{-9} (*Picea abies*) at MIT. ^{10}Be(meteoric)/^{9}Be ratios found in leaf foliage exceed those found in wood (CON: 5.0×10^{-9} (*Picea abies*) and 7.8×10^{-9} (*Fagus sylvatica*), MIT: 7.7×10^{-9} (*Fagus sylvatica*)) with the exception for *Picea abies* at MIT, where ^{10}Be(meteoric)/^{9}Be found in wood are 19×10^{-9} (Figure 3, Table S4). That the ^{10}Be(meteoric)/

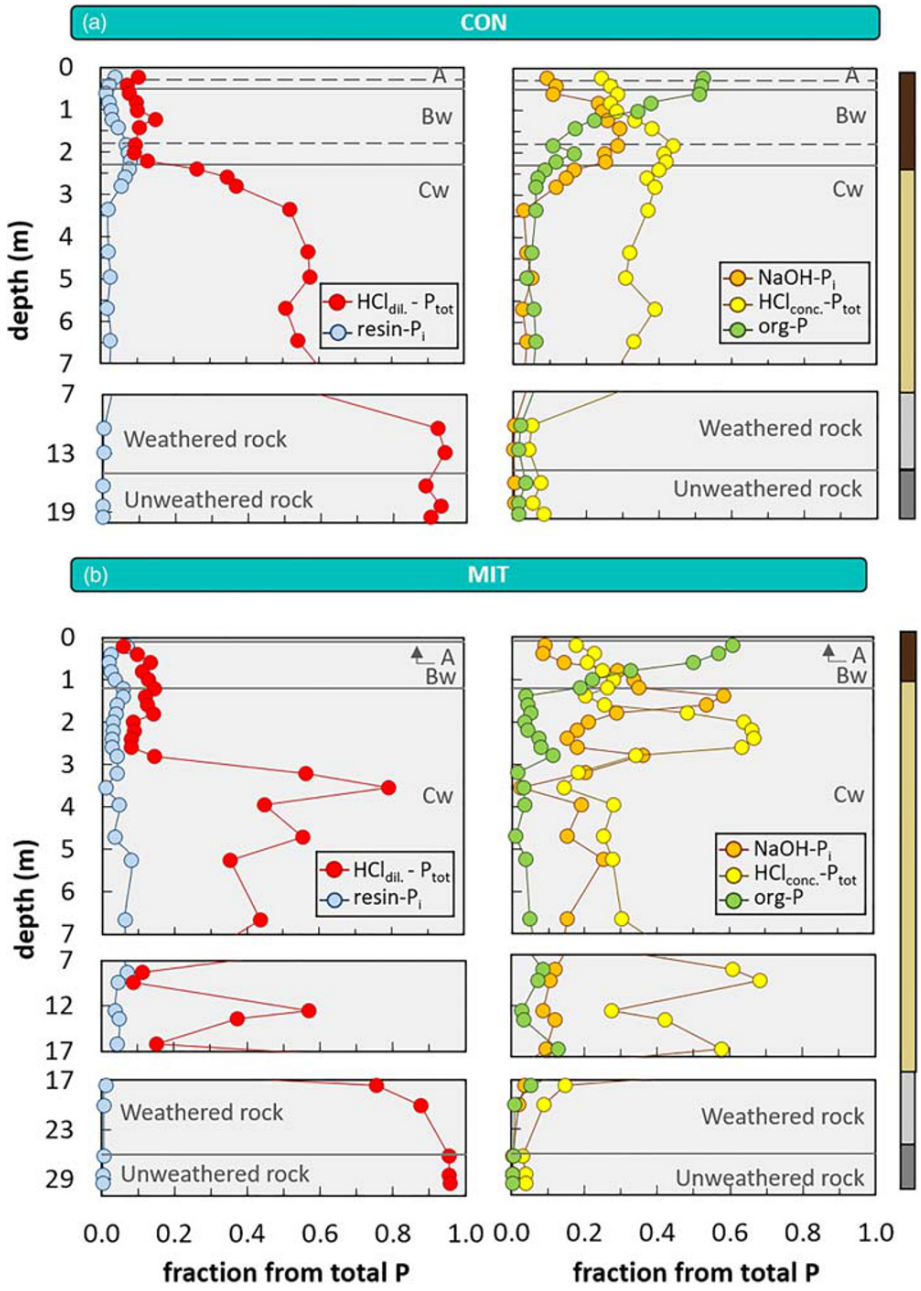

Figure 4. Depth distribution of selected extractable phosphorus (P) fractions relative to total P at each depth (Hedley fractionation, see section 4) at CON (panel a) and MIT (panel b). Extracted P fractions correspond to figure legends (see Table 1 for detailed descriptions). Left-hand panels show (potentially) biologically available fractions and right-hand panels show less and non-biologically available fractions. The $NaHCO_3$-extractable P_i form is not shown. A, Bw, Cw: Soil horizons. Stippled lines subdivide soil horizons (A into Ah and Ah + Bw, B into Bw1 and Bw2). Colored bars at the right side of panels (a) and (b) assign data to soil (brown), saprolite (beige), weathered rock (light gray), unweathered rock (dark gray). Note the change in *y*-axis spacing with depth, yet all data are shown continuously. One sample from 1.6 m depth at CON was excluded after performing a Grubbs outlier test.

^{9}Be ratio of foliage exceeds the ^{10}Be/^{9}Be ratio in wood is due to the direct uptake of wet deposition, which is rich in ^{10}Be(meteoric), through leaf stomata. This effect is more pronounced for coniferous than for deciduous species due to the higher relative surface area and the longer lifetime of its foliage. We thus compare the wood ^{10}Be(meteoric)/^{9}Be ratio with the am-ox ratio to fingerprint the nutrient uptake depth. The ^{10}Be(meteoric)/^{9}Be of *Fagus sylvatica* matches the am-ox ratio at 1.5 to 2.0 m depth at CON and at 0.0 to

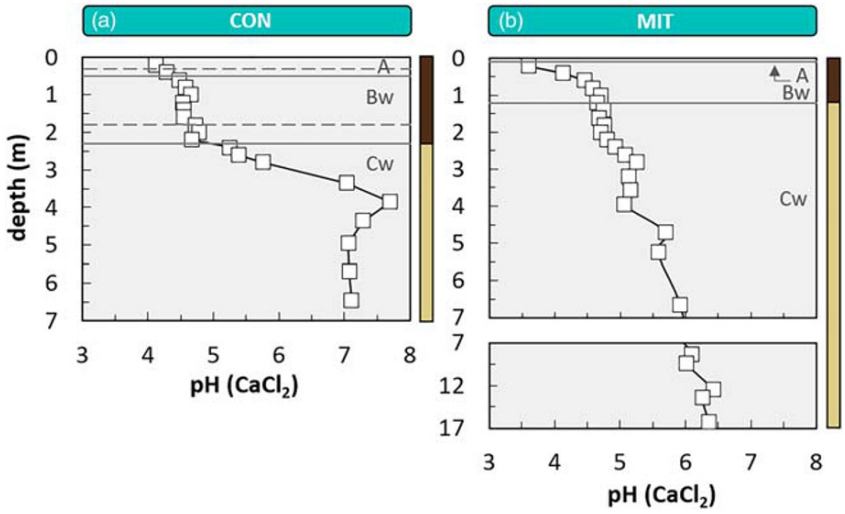

Figure 5. Depth distributions of soil pH at CON (panel a) and MIT (panel b). A, Bw, Cw: Soil horizons. Horizontal stippled lines subdivide soil horizons (A into Ah and Ah + Bw, B into Bw1 and Bw2). Colored bars at the right side of panels (a) and (b) assign data to soil (brown) and saprolite (beige). Note that for ease of display, *y*-axis scaling at MIT changes beyond 7 m depth.

1.5 m depth at MIT, and *Picea abies* at 2.0 to 3.5 m depth at CON and 1.5 to 2.5 m depth at MIT (Figure 3, Tables S4 and S5). Given these differences, the uptake depth of Be is apparently species dependent.

5.3. Phosphorus Availability With Depth

Hedley sequential phosphorus fractionation was performed to evaluate the biological availability of P with depth. The depth distribution of P forms show that P in soil regolith consists mainly of P in the occluded form (relative to total P up to 42% at CON and up to 28% at MIT) and recalcitrant form (relative to total P up to 29% at CON and 35% at MIT) (Figure 4, Table S6) that are essentially unavailable to direct utilization by forest trees. A potentially biologically available form of P (calcium-bound HCl_{dil}-P_i) is the dominant extractable P form only in deep saprolite and weathered bedrock at 7 m and 17 m depth at CON and MIT. Thus, at both study sites, a considerable fraction of potentially biologically available calcium-bound P is present only in the deep saprolite (*in situ* bedrock that has experienced strong weathering) and bedrock that was weathered along fractures.

6. Discussion

6.1. Nutrient Uptake Depth

We compared the $^{87}Sr/^{86}Sr$ ratio and, for the first time, the $^{10}Be(meteoric)/^{9}Be$ ratio in forest trees to the biologically available fraction in the regolith as a fingerprint of uptake depth. We interpret these to denote the uptake depth of the mono- and divalent mineral nutrients. The uptake depth differs between Sr and Be, likely caused by the differential mobility of these elements within the regolith depth profile. In the presence of organic compounds that resemble humic acid, Be is strongly bound to solid surfaces at a soil pH above 4 (Willenbring & von Blanckenburg, 2010). In the absence of humic acid, Be is bound at a soil pH above 6 (Willenbring & von Blanckenburg, 2010). Beryllium is thus predicted to be retained in the organic carbon-rich topsoil up to ~1.5 m where soil pH is >4 at both sites. Beryllium is also retained below ~3 m depth at CON and ~8 m at MIT where the soil pH is >6 (Figure 5, Table S1). These predictions allow us to infer that Be is mobile only in the depth range of 1.5 to 3 m at CON and to 8 m at MIT. In contrast, Sr is mobile at both acidic and neutral pH. This pH range is found at both sites throughout the soil-saprolite profile (Figure 5). Thus, Sr tracks a deeper uptake depth for the metals Ca, K, and Mg (see section 2.2) than beryllium. The uptake depth obtained from $^{10}Be(meteoric)/^{9}Be$ hence presents a minimum depth for their uptake depth. The deep uptake indicated by Sr is likely also indicative for P uptake because a soil pH of 6 to 7 provides the highest solubility of the potentially biologically available calcium phosphate in the regolith (Brady & Weil, 2002). Recent data by Rodionov et al. (2020, in press) indicate biologically mediated oxygen

isotope exchange in PO_4 up to a depth of 3.4 at MIT and to 4.7 m at CON. We can confirm conditions favorable to mobilization of both P and Sr deep in the profiles. The soil pH ranges between 6 and pH 7 at ~3 m and 5–7 m at CON, and at 7–17 m at MIT (Figure 5, Table S1). Thus, the uptake depth of Be at MIT and for *Fagus sylvatica* at CON is shallower than that of Sr (Figure 5). In any case we find evidence for the upward translocation of mineral-sourced K, Ca, and Mg from 2–17 m depth, and it is likely that P is among them as P occurs in potentially biologically available form only in substantial amounts at depths below 2 m (Figure 4).

6.2. Atmospheric Dust Deposition—An Alternative Nutrient Source?

An alternative explanation for forest ecosystems to sustain millennial scale nutrition is nutrient utilization from atmospheric dust deposition. For example, Aciego et al. (2017) suggested that for the most plant-essential mineral nutrient P supply by atmospheric dust deposition outpaces P supply from local bedrock, a conclusion contested for the P-rich bedrock site in that study by Uhlig et al. (2017). Arvin et al. (2017) underpinned the Aciego et al. (2017) argument by comparing P release from regolith with P input from Last Glacial Maximum (LGM) dust that is thought to having exceeded the modern dust flux in many parts of the Earth. However, using erosion rates reported in Uhlig and von Blanckenburg (2019a) and bulk soil densities (Bw soil horizon) provided by F. Lang (personal communication, reported in Uhlig & von Blanckenburg, 2019a) from CON and MIT reveals that since LGM about 60 cm of soil would have been eroded at CON and about 75 cm at MIT, which means that any remaining solid LGM P would have been eroded since then.

Apparently in favor of the dust hypothesis, the radiogenic Sr isotope composition of forest trees at CON and MIT fall within the range found for potential source areas of atmospheric dust in the Sahara and Asian desert. Specifically, at both sites $^{87}Sr/^{86}Sr$ of living leaf foliage and wood ranges from 0.714 to 0.718, whereas $^{87}Sr/^{86}Sr$ of Saharan dust ranges from 0.711 to 0.754 (Gross et al., 2016) and Asian dust ranges from 0.715 to 0.748 (Grousset & Biscaye, 2005). Despite this isotope match, three lines of evidence still suggest it is unlikely that atmospheric dust contributes substantially to long-term forest ecosystem nutrition at CON and MIT. First, neither the distribution of element concentrations (provided in Uhlig & von Blanckenburg, 2019a) nor $^{87}Sr/^{86}Sr$ ratios with depth show a clear indication for substantial atmospheric dust deposition at both study sites. Second, estimates of dust deposition fluxes (Dep^{X}_{dust}, section 4.2.7, Table 2) of plant essential mineral nutrients (K: 37–150, Ca: 54–180, Mg: 21–73, P: 1.3–4.8; all in mg m^{-2} $year^{-1}$) are much lower than nutrient supply fluxes by rock weathering (CON: K: 1,000, Ca: 5,500, Mg: 2,000, P: 84; MIT: K: 240, Ca: 980, Mg: 400, P: 65; all in mg m^{-2} $year^{-1}$; Table 2). Also atmospheric wet deposition fluxes (CON: K: 160, Ca: 380, Mg: 53, P: 7.1; MIT: K: 340, Ca: 370, Mg: 73, P: 46; all in mg m^{-2} $year^{-1}$; Table 2) are lower than nutrient supply by rock weathering at CON and at MIT (where measured atmospheric deposition is likely dominated by anthropogenic inputs today, Uhlig & von Blanckenburg, 2019a). Hence, dust deposition is insufficient to balance the annual loss fluxes of mineral nutrients at our study sites. Third, the data for Dep^{X}_{dust} represent likely an overestimate because it contains local soil material (e.g., Lequy et al., 2012), which should be considered as an internal rather than an external input to the forest ecosystem.

Given these arguments we believe that nutrient utilization from depth is a more likely process to sustain long-term forest ecosystem nutrition than the supply of atmospheric dust at CON and MIT and possibly at other sites globally with similar dust fluxes, denudation rates, and parent lithology.

6.3. Nutrient Uplift Pathways

Given the collective evidence provided above we suggest that the balance of permanent loss of organic-bound mineral nutrients over their residence time in soil is achieved by nutrient uptake from depth, that is, nutrient uplift (Bullen & Chadwick, 2016; Jobbágy & Jackson, 2004). The differences in the uptake depth of the elements Sr and Be (interpreted to constrain the range of uptake depth of the mineral-derived nutrients K, Ca, Mg, and P) provide an insight into the uplift pathways that we infer to be several meters long. The most obvious mechanism is direct uptake by roots. *Picea abies* is known to root shallowly, particularly in mixed stands with *Fagus sylvatica* (Schmid & Kazda, 2002), where *Fagus sylvatica* acts as a Ca-pump for *Picea abies* (Berger et al., 2006). Our results suggest nutrient uptake from a depth beyond the mean rooting depth of *Picea* or *Fagus* (0.74 ± 0.47 m [$N = 80$] and 0.83 ± 0.46 m [$N = 8$] respectively; Fan et al., 2017), and beyond the estimated maximum rooting depth of *Picea abies* and *Fagus sylvatica* in European forests of less than 2 m (e.g., Canadell et al., 1996; Claus & George, 2005; Drexhage &

Gruber, 1998; Schmid & Kazda, 2005). Hence, this nutrient uplift would need to be mediated by a few roots that grow much deeper than the maximum root length suggests. Indeed, it has previously been suggested that for water storage and uptake into the shallow rooting zone trees may rely on the few roots reaching much deeper, which in surveys of rooting depth are likely undersampled (Fan et al., 2017). Plant rooting depth is regulated hydrologically and is often strongly correlated with the depth of the groundwater water table (Fan et al., 2017). Dimorphic root systems (comprising shallow horizontal roots and deep taproots) allow trees to tap into the capillary fringe near the water table (Fan et al., 2017). In doing so, for example, during summer droughts, they likely simultaneously take up mobilized mineral nutrients. Although varying seasonally, the water table lies at 7.5 m depth at site CON and at 8 m depth at site MIT, which is consistent with the uptake depth inferred from $^{87}Sr/^{86}Sr$ (Figure 2) as well as with the most significant increase of potentially biologically available calcium-phosphate with depth (Figure 4). Hydraulic redistribution by roots (Lambers et al., 2006; McCulley et al., 2004) reallocates deep water (potentially carrying dissolved nutrients) from deep soil horizons to shallow roots.

Despite the good agreement between nutrient source depth and the position of the water table at our sites, since we still lack visual evidence for the presence of roots at depths of ~8 m within our drill cores, it is possible that capillary rise and diffusion are additional nutrient uplift mechanisms. This abiotic lift may further be supported by hyphae of endomycorrhiza fungi that can bridge deep nutrient sources and shallow tree roots by more than a meter (Graham et al., 2010). Such hyphae have been found to extend in oak woodland down to 4 m depth (Bornyasz et al., 2005; Querejeta et al., 2007) and up to 6 m in Eucalypt plantation (Santana et al., 2016). At that depth, hyphae take up nutrient-rich pore waters or in the case of P penetrate directly into mineral grains, such as apatite, for nutrient uptake (Bornyasz et al., 2005; Schmitt et al., 2017). We suggest therefore that a combination of root-mycorrhizal symbiosis, dimorphic root systems, and capillary rise (Figure 1) may be involved in nutrient uplift from depth. This finding provides evidence that organic-bound nutrient losses from an ecosystem can be balanced through nutrient uptake from a deep reservoir that is rich in biologically available nutrients (for P see Figure 4; for Ca, K, and Mg see Uhlig & von Blanckenburg, 2019a) and which can then be cycled multiple times through the forest floor and trees.

6.4. Global Implications and Limitations

Cleveland et al. (2013) estimated that up to about 6% of plant P uptake takes place from so-called "new" P, defined as P that is not recycled from organic matter, but is instead taken up freshly from regolith. Given our isotope-derived evidence that organic-bound nutrients originally entered the organic nutrient cycle after uptake from a deep and biologically available nutrient reservoir, we suggest that some of this "new" uptake might also stem from a deep source (in regions where atmospheric inputs are insufficient to balance the geogenic nutrient cycle). This deep nutrient uptake may be particularly relevant in the half of the terrestrial surface in which slopes exceed 5°, and thus experience slow, but permanent erosion. Such erosion ensures that fresh minerals are advected into a regolith depth that is in principle, as we show, accessible to forest trees.

This deep nutrient uptake mechanism is likely significant in temperate forest ecosystems with gentle to moderate hillslopes and rainfall but may not necessarily play a key role in forest ecosystems with very steep hillslopes in areas of high rainfall, for example, in steep sloping tropical rainforests. These ecosystems are frequently affected by mass wasting events such as landslides or soil avalanches (e.g., Larsen, 2012; Stallard, 1995, 2012), meaning that rejuvenation of weathering-derived nutrient supply takes place frequently enough that re-established forest trees would not need to access deep, less weathered regolith layers to sustain forest ecosystem function. Yet, in many tropical areas also, root systems may reach up to 18 m depth (Nepstad et al., 1994). Thus, quantifying nutrient uplift from depth in such areas may warrant attention too.

Finally, deep nutrient uptake may not prevail in forest ecosystems located on very flat or non-sloping landscapes. These settings are characterized by intensely weathered regolith of up to 100 m thickness (e.g., Richter & Markewitz, 1995). In this case the nutrient-rich weathering front would almost certainly be beyond the reach of tree roots. However, a key difference between very flat or non-sloping landscapes and gently or moderately sloping landscapes is that annual nutrient loss by erosion and drainage is likely very low and that recycling of organic-bound nutrients is very efficient (Chadwick et al., 1999; Lambers et al., 2011; Schuessler et al., 2018; Wilcke et al., 2002). In such settings, nutrient inputs by atmospheric deposition

sustain primary productivity on the millennial timescale (e.g., Chadwick et al., 1999), thereby continuously balances the only minor nutrient loss from the ecosystem.

7. Conclusions

We applied the isotope ratio of radiogenic Sr ($^{87}Sr/^{86}Sr$) and, for the first time, the isotope ratio of cosmogenic meteoric Be ($^{10}Be(meteoric)/^{9}Be$) as proxies for nutrient uptake depth. These proxies indicate two distinct nutrient uptake depths. On the one hand, the $^{87}Sr/^{86}Sr$ isotope ratios in living tree tissue and organic matter matched the biologically available fraction in the forest floor and topsoil. This agreement implicates the "organic nutrient pathway," that is, the efficient recycling of nutrients from the forest floor as largest supplier of mineral nutrients to forest trees. However, flux balances indicate that the forest floor pool will be depleted by nutrient losses within centuries. This loss must be balanced by uptake from regolith. We thus used these tracers to explore from what depth the compensatory source of, for example, phosphorus and other mineral nutrients is acquired. $^{10}Be(meteoric)/^{9}Be$ revealed this depth to lie within the top 2.5 m, and to differ between species. For the radiogenic $^{87}Sr/^{86}Sr$ ratio, which refers to the uptake depth of K, Ca and Mg, we found this depth to lie below 2 m and potentially up to 17 m. Because potentially biologically available calcium phosphate is also present in substantial amounts from about 3 m depth down to parent bedrock, we regard it as likely that P is also sourced from this depth interval. These findings provide evidence that organic-bound nutrient losses from the forest floor are not necessarily balanced by supply from external atmospheric dust deposition, but rather through nutrient uptake from a deep reservoir that is rich in biologically available mineral nutrients—the "geogenic nutrient pathway." We suggest that biogeochemical and linked hydrological transfers taking place in subsoil and the deep saprolite are an important missing link in ecosystem nutrition and that these pathways warrant greater consideration within the field.

Data Availability Statement

The data set including Tables S1–S6 of this study is accessible in the data repository under the reference Uhlig et al. (2020).

Acknowledgments

We are grateful for funding from the German National Science Foundation Priority Program 1685 "Ecosystem nutrition: forest strategies for limited phosphorus resources" and to Friederike Lang for coordination and discussions. We also thank the Bayerische Landesanstalt für Wald und Forstwirtschaft (LWF) and the Forstliche Versuchsanstalt Baden-Wuerttemberg (FVA) for providing wet deposition data. R. Naumann (GFZ) and A. Gottsche (GFZ) are acknowledged for X-ray fluorescence and X-ray diffraction analyses. We thank J. Schuessler (GFZ), H. Wittmann (GFZ) and G. Floor (GFZ) for analytical support. R. Kapannusch (GFZ) as well as A. Rodionov and S. Bauke (University of Bonn, INRES) are acknowledged for field work, sample preparation and analyses. We thank J. Caves Rugenstein, M. Spohn, P. Frings, F. Hagedorn und F. Lang for discussions and reviews of an early version of this manuscript. Robert F. Stallard and two anonymous reviewers are acknowledged for constructive and critical reviews, which helped to improve this manuscript.

References

Åberg, G., Jacks, G., Wickman, T., & Hamilton, P. J. (1990). Strontium isotopes in trees as an indicator for calcium availability. *Catena*, *17*(1), 1–11. https://doi.org/10.1016/0341-8162(90)90011-2

Aciego, S. M., Riebe, C. S., Hart, S. C., Blakowski, M. A., Carey, C. J., Aarons, S. M., et al. (2017). Dust outpaces bedrock in nutrient supply to montane forest ecosystems. *Nature Communications*, *8*, 1–10. https://doi.org/10.1038/ncomms14800

Ackermann, S., Amelung, W., & Löffler, J. (2015). Additional nitrogen in arctic-alpine soils and plants—A pilot study with $^{15}NO_3^-$ and $^{15}NH_4^+$ fertilization along an elevation gradient. *Journal of Plant Nutrition and Soil Science*, *178*(6), 861–867. https://doi.org/10.1002/jpln.201500008

Arvin, L. J., Riebe, C. S., Aciego, S. M., & Blakowski, M. A. (2017). Global patterns of dust and bedrock nutrient supply to montane ecosystems. *Science Advances*, *3*(12), eaao1588–11. https://doi.org/10.1126/sciadv.aao1588

Augusto, L., Achat, D. L., Jonard, M., Vidal, D., & Ringeval, B. (2017). Soil parent material—A major driver of plant nutrient limitations in terrestrial ecosystems. *Global Change Biology*, *23*(9), 3808–3824. https://doi.org/10.1111/gcb.13691

Avila, A., Alarcón, M., & Queralt, I. (1998). The chemical composition of dust transported in red rains - its contribution to the biogeochemical cycle of a Holm Oak Forest in Catalonia (Spain). *Atmospheric Environment*, *32*(2), 179–191. https://doi.org/10.1016/S1352-2310(97)00286-0

Bacon, A. R., Richter, D. D., Bierman, P. R., & Rood, D. H. (2012). Coupling meteoric ^{10}Be with pedogenic losses of ^{9}Be to improve soil residence time estimates on an ancient North American interfluve. *Geology*, *40*(9), 847–850. https://doi.org/10.1130/G33449.1

Bacon, J. R., & Davidson, C. M. (2008). Is there a future for sequential chemical extraction? *The Analyst*, *133*(1), 25–46. https://doi.org/10.1039/B711896A

Bailey, S. W., Hornbeck, J. W., Driscoll, C. T., & Gaudette, E. (1996). Calcium inputs and transport in a base-poor forest ecosystem as interpreted by Sr isotopes sample. *Water Resources Research*, *32*(3), 707–719. https://doi.org/10.1029/95WR03642

Barej, J. A. M., Pätzold, S., Perkons, U., & Amelung, W. (2014). Phosphorus fractions in bulk subsoil and its biopore systems. *European Journal of Soil Science*, *65*(4), 553–561. https://doi.org/10.1111/ejss.12124

Baxter, S. (2007). World Reference Base for Soil Resources. World Soil Resources Report 103. Rome: Food and Agriculture Organization of the United Nations (2006), pp. 132, US$22.00 (paperback). *Experimental Agriculture*, *43*(2), 264–264. https://doi.org/10.1017/s0014479706394902

Becker, G. F. (1895). *Reconnaissance of the gold fields of the southern Appalachians*. U.S. Geological Survey: U.S. Government Printing Office.

Bedel, L., Poszwa, A., van der Heijden, G., Legout, A., Aquilina, L., & Ranger, J. (2016). Unexpected calcium sources in deep soil layers in low-fertility forest soils identified by strontium isotopes (Lorraine plateau, eastern France). *Geoderma*, *264*, 103–116. https://doi.org/10.1016/j.geoderma.2015.09.020

Bélanger, N., Holmden, C., Courchesne, F., Côté, B., & Hendershot, W. H. (2012). Constraining soil mineral weathering $^{87}Sr/^{86}Sr$ for calcium apportionment studies of a deciduous forest growing on soils developed from granitoid igneous rocks. *Geoderma*, *185-186*, 84–96. https://doi.org/10.1016/j.geoderma.2012.03.024

Berger, T. W., Swoboda, S., Prohaska, T., & Glatzel, G. (2006). The role of calcium uptake from deep soils for spruce (*Picea abies*) and beech (*Fagus sylvatica*). *Forest Ecology and Management*, *229*(1–3), 234–246. https://doi.org/10.1016/j.foreco.2006.04.004

Blecker, S. W., King, S. L., Derry, L. A., Chadwick, O. A., Ippolito, J. A., & Kelly, E. F. (2007). The ratio of germanium to silicon in plant phytoliths: Quantification of biological discrimination under controlled experimental conditions. *Biogeochemistry*, *86*(2), 189–199. https://doi.org/10.1007/s10533-007-9154-7

Blum, J. D., Dasch, A. A., Hamburg, S. P., Yanai, R. D., & Arthur, M. A. (2008). Use of foliar Ca/Sr discrimination and $^{87}Sr/^{86}Sr$ ratios to determine soil Ca sources to sugar maple foliage in a northern hardwood forest. *Biogeochemistry*, *87*(3), 287–296. https://doi.org/10.1007/s10533-008-9184-9

Blum, J. D., Hamburg, S. P., Yanai, R. D., & Arthur, M. A. (2012). Determination of foliar Ca/Sr discrimination factors for six tree species and implications for Ca sources in northern hardwood forests. *Plant and Soil*, *356*(1–2), 303–314. https://doi.org/10.1007/s11104-011-1122-2

Blum, J. D., Klaue, A., Nezat, C. A., Driscoll, C. T., Johnson, C. E., Siccama, T. G., et al. (2002). Mycorrhizal weathering of apatite as an important calcium source in base-poor forest ecosystems. *Nature*, *417*(6890), 729–731. https://doi.org/10.1038/nature00793

Bol, R., Julich, D., Brödlin, D., Siemens, J., Kaiser, K., Dippold, M. A., et al. (2016). Dissolved and colloidal phosphorus fluxes in forest ecosystems—An almost blind spot in ecosystem research. *Journal of Plant Nutrition and Soil Science*, *179*(4), 425–438. https://doi.org/10.1002/jpln.201600079

Bornyasz, M. A., Graham, R. C., & Allen, M. F. (2005). Ectomycorrhizae in a soil-weathered granitic bedrock regolith: Linking matrix resources to plants. *Geoderma*, *126*, 141–160. https://doi.org/10.1016/j.geoderma.2004.11.023

Brady, N. C., & Weil, R. R. (2002). The nature and properties of soils, 13th. Pearson Education (Singapore) Pte. Ltd. *Indian Branch*, *482*, 621–624.

Brown, E. T., Edmond, J. M., Raisbeck, G. M., Bourlès, D. L., Yiou, F., & Measures, C. I. (1992). Beryllium isotope geochemistry in tropical river basins. *Geochimica et Cosmochimica Acta*, *56*(4), 1607–1624. https://doi.org/10.1016/0016-7037(92)90228-B

Bullen, T., & Chadwick, O. (2016). Ca, Sr and Ba stable isotopes reveal the fate of soil nutrients along a tropical climosequence in Hawaii. *Chemical Geology*, *422*, 25–45. https://doi.org/10.1016/j.chemgeo.2015.12.008

Bullen, T. D., & Bailey, S. W. (2005). Identifying calcium sources at an acid deposition-impacted spruce forest: A strontium isotope, alkaline earth element multi-tracer approach. *Biogeochemistry*, *74*(1), 63–99. https://doi.org/10.1007/s10533-004-2619-z

Canadell, J., Jackson, R. B., Ehleringer, J. B., Mooney, H. A., Sala, O. E., & Schulze, E.-D. (1996). Maximum rooting depth of vegetation types at the global scale. *Oecologia*, *108*(4), 583–595. https://doi.org/10.1007/BF00329030

Castillo, S., Moreno, T., Querol, X., Alastuey, A., Cuevas, E., Herrmann, L., et al. (2008). Trace element variation in size-fractionated African desert dusts. *Journal of Arid Environments*, *72*(6), 1034–1045. https://doi.org/10.1016/j.jaridenv.2007.12.007

Chadwick, O. A., Derry, L. A., Vitousek, P. M., Huebert, B. J., & Hedin, L. O. (1999). Changing sources of nutrients during four million years of ecosystem development. *Nature*, *397*(6719), 491–497. https://doi.org/10.1038/17276

Chapin, F. S. III, & Van Cleve, K. (2000). Approaches to studying nutrient uptake, use and loss in plants. In *Plant physiological ecology* (pp. 185–207). Dordrecht: Springer. https://doi.org/10.1007/978-94-010-9013-1_10

Claus, A., & George, E. (2005). Effect of stand age on fine-root biomass and biomass distribution in three European forest chronosequences. *Canadian Journal of Forest Research*, *35*(7), 1617–1625. https://doi.org/10.1139/x05-079

Cleveland, C. C., Houlton, B. Z., Smith, W. K., Marklein, A. R., Reed, S. C., Parton, W., et al. (2013). Patterns of new versus recycled primary production in the terrestrial biosphere. *Proceedings of the National Academy of Sciences*, *110*(31), 12,733–12,737. https://doi.org/10.1073/pnas.1302768110

Cleveland, C. C., Reed, S. C., & Townsend, A. R. (2006). Nutrient regulation of organic matter decomposition in a tropical rain forest. *Ecology*, *87*(2), 492–503. https://doi.org/10.1890/05-0525

Coble, A. A., Hart, S. C., Ketterer, M. E., Newman, G. S., & Kowler, A. L. (2015). Strontium source and depth of uptake shifts with substrate age in semiarid ecosystems. *Journal of Geophysical Research: Biogeosciences*, *120*, 1069–1077. https://doi.org/10.1002/2015JG002992. Received

Cross, A. F., & Schlesinger, W. H. (1995). A literature review and evaluation of the Hedley fractionation: Applications to the biogeochemical cycle of soil phosphorus in natural ecosystems. *Geoderma*, *64*(3–4), 197–214. https://doi.org/10.1016/0016-7061(94)00023-4

Dannhaus, N., Wittmann, H., Krám, P., Christl, M., & von Blanckenburg, F. (2018). Catchment-wide weathering and erosion rates of mafic, ultramafic, and granitic rock from cosmogenic meteoric $^{10}Be/^{9}Be$ ratios. *Geochimica et Cosmochimica Acta*, *222*, 618–641. https://doi.org/10.1016/j.gca.2017.11.005

Dawson, T. E., Hahm, W. J., & Crutchfield-Peters, K. (2020). Digging deeper: What the critical zone perspective adds to the study of plant ecophysiology. *New Phytologist*, *226*(3), 666–671. https://doi.org/10.1111/nph.16410

De Angelis, M., & Gaudichet, A. (1991). Saharan dust deposition over Mont Blanc (French Alps) during the last 30 years. *Tellus*, *43B*, 61–75.

De Oliveira Garcia, W., Amann, T., & Hartmann, J. (2018). Increasing biomass demand enlarges negative forest nutrient budget areas in wood export regions. *Scientific Reports*, *8*(1), 5280. https://doi.org/10.1038/s41598-018-22728-5

Delvigne, C., Opfergelt, S., Cardinal, D., Delvaux, B., & André, L. (2009). Distinct silicon and germanium pathways in the soil-plant system: Evidence from banana and horsetail. *Journal of Geophysical Research*, *114*, G02013. https://doi.org/10.1029/2008JG000899

Derry, L. A., Kurtz, A. C., Ziegler, K., & Chadwick, O. A. (2005). Biological control of terrestrial silica cycling and export fluxes to watersheds. *Nature*, *433*(7027), 728–731. https://doi.org/10.1038/nature03299

Drexhage, M., & Gruber, F. (1998). Architecture of the skeletal root system of 40-year-old *Picea abies* on strongly acidified soils in the Harz Mountains (Germany). *Canadian Journal of Forest Research*, *28*(1), 13–22. https://doi.org/10.1139/x97-181

Drouet, T., & Herbauts, J. (2008). Evaluation of the mobility and discrimination of Ca, Sr and Ba in forest ecosystems: Consequence on the use of alkaline-earth element ratios as tracers of Ca. *Plant and Soil*, *302*(1–2), 105–124. https://doi.org/10.1007/s11104-007-9459-2

Drouet, T., Herbauts, J., & Demaiffe, D. (2005). Long-term records of strontium isotopic composition in tree rings suggest changes in forest calcium sources in the early 20th century. *Global Change Biology*, *11*(11), 1926–1940. https://doi.org/10.1111/j.1365-2486.2005.01034.x

Drouet, T., Herbauts, J., Gruber, W., & Demaiffe, D. (2005). Strontium isotope composition as a tracer of calcium sources in two forest ecosystems in Belgium. *Geoderma*, *126*(3–4), 203–223. https://doi.org/10.1016/j.geoderma.2004.09.010

Du, E., Terrer, C., Pellegrini, A. F. A., Ahlström, A., van Lissa, C. J., Zhao, X., et al. (2020). Global patterns of terrestrial nitrogen and phosphorus limitation. *Nature Geoscience*, *13*(3), 221–226. https://doi.org/10.1038/s41561-019-0530-4

Fan, Y., Miguez-Macho, G., Jobbágy, E. G., Jackson, R. B., & Otero-Casal, C. (2017). Hydrologic regulation of plant rooting depth. *Proceedings of the National Academy of Sciences*, *114*(40), 10,572–10,577, 1–6. https://doi.org/10.1073/pnas.1712381114

Faure, G., & Mensing, T. M. (2005). *Isotopes: Principles and applications*, Oxford, UK: John Wiley & Sons, Inc.

Fernández-Martínez, M., Vicca, S., Janssens, I. A., Sardans, J., Luyssaert, S., Campioli, M., et al. (2014). Nutrient availability as the key regulator of global forest carbon balance (Suppl.). *Nature Climate Change*, *4*(6), 471–476. https://doi.org/10.1038/nclimate2177

Filgueiras, A. V., Lavilla, I., & Bendicho, C. (2002). Chemical sequential extraction for metal partitioning in environmental solid samples. *Journal of Environmental Monitoring*, *4*(6), 823–857. https://doi.org/10.1039/b207574c

Germon, A., Laclau, J. P., Robin, A., & Jourdan, C. (2020). Tamm review: Deep fine roots in forest ecosystems: Why dig deeper? *Forest Ecology and Management*, *466*(April), 118135. https://doi.org/10.1016/j.foreco.2020.118135

Gottselig, N., Sohrt, J., Uhlig, D., Nischwitz, V., Weiler, M., & Amelung, W. (2020). Groundwater controls on colloidal transport in forest stream waters. *Science of The Total Environment.*, *717*, 134638. https://doi.org/10.1016/j.scitotenv.2019.134638

Goudie, A. S., & Middleton, N. J. (2001). Saharan dust storms: Nature and consequences. *Earth-Science Reviews*, *56*(1–4), 179–204. https://doi.org/10.1016/S0012-8252(01)00067-8

Graham, R. C., Rossi, A. M., & Hubbert, K. R. (2010). Rock to regolith conversion: Producing hospitable substrates for terrestrial ecosystems. *GSA Today*, *20*(2), 4–9. https://doi.org/10.1130/GSAT57A.1

Gross, A., Palchan, D., Krom, M. D., & Angert, A. (2016). Elemental and isotopic composition of surface soils from key Saharan dust sources. *Chemical Geology*, *442*, 54–61. https://doi.org/10.1016/j.chemgeo.2016.09.001

Grousset, F. E., & Biscaye, P. E. (2005). Tracing dust sources and transport patterns using Sr, Nd and Pb isotopes. *Chemical Geology*, *222*(3–4), 149–167. https://doi.org/10.1016/j.chemgeo.2005.05.006

Guelke, M., von Blanckenburg, F., Schoenberg, R., Staubwasser, M., & Stuetzel, H. (2010). Determining the stable Fe isotope signature of plant-available iron in soils. *Chemical Geology*, *277*(3–4), 269–280. https://doi.org/10.1016/j.chemgeo.2010.08.010

Heartsill Scalley, T., Scatena, F. N., Moya, S., & Lugo, A. E. (2012). Long-term dynamics of organic matter and elements exported as coarse particulates from two Caribbean montane watersheds. *Journal of Tropical Ecology*, *28*(2), 127–139. https://doi.org/10.1017/S0266467411000733

Hedley, M. J., Stewart, J. W. B., & Chauhan, B. S. (1982). Changes in inorganic and organic soil phosphorus fractions induced by cultivation practices and by laboratory incubations1. *Soil Science Society of America Journal*, *46*(5), 970–976. https://doi.org/10.2136/sssaj1982.03615995004600050017x

Helfenstein, J., Tamburini, F., von Sperber, C., Massey, M. S., Pistocchi, C., Chadwick, O. A., et al. (2018). Combining spectroscopic and isotopic techniques gives a dynamic view of phosphorus cycling in soil. *Nature Communications*, *9*(1), 3226–3229. https://doi.org/10.1038/s41467-018-05731-2

Hewawasam, T., von Blanckenburg, F., Bouchez, J., Dixon, J. L., Schuessler, J. A., & Maekeler, R. (2013). Slow advance of the weathering front during deep, supply-limited saprolite formation in the tropical highlands of Sri Lanka. *Geochimica et Cosmochimica Acta*, *118*, 202–230. https://doi.org/10.1016/j.gca.2013.05.006

Hladil, J., Strnad, L., Šálek, M., Jankovská, V., Šimandl, P., Schwarz, J., et al. (2008). An anomalous atmospheric dust deposition event over Central Europe, 24 March 2007, and fingerprinting of the SE Ukrainian source. *Bulletin of Geosciences*, *83*(2), 175–206. https://doi.org/10.3140/bull.geosci.2008.02.175

Holden, N. E. (1990). Total half-lives for selected nuclides. *International Union of Pure and Applied Chemistry*, *62*(5), 941–958. https://doi.org/10.1351/pac199062050941, http://pmd.gfz-potsdam.de/panmetaworks/review/20e6316d7f0906ac2cd0c8a23a6e07798b64bc65a7f0912ca01aafe26787b48b/

Jackson, R. B., Banner, J. L., Jobbaágy, E. G., Pockman, W. T., & Wall, D. H. (2002). Ecosystem carbon loss with woody plant invasion of grasslands. *Nature*, *418*(6898), 623–626. https://doi.org/10.1038/nature00910

Jickells, T. D., An, Z. S., Andersen, K. K., Baker, A. R., Bergametti, G., Brooks, N., et al. (2005). Global iron connections between desert dust, ocean biogeochemistry, and climate. *Science*, *308*(5718), 67–71. https://doi.org/10.1126/science.1105959

Jobbagy, E. G., & Jackson, R. B. (2000). The vertical distribution of soil organic carbon and its relation to climate and vegetation. *Ecological Applications*, *10*(2), 423–436. https://doi.org/10.2307/2641104

Jobbágy, E. G., & Jackson, R. B. (2001). The distribution of soil nutrients with depth: Global patterns and the imprint of plants. *Biogeochemistry*, *53*(1), 51–77. https://doi.org/10.1023/A:1010760720215

Jobbágy, E. G., & Jackson, R. B. (2004). The uplift of soil nutrients by plants: Biogeochemical consequences across scales. *Ecology*, *85*(9), 2380–2389. https://doi.org/10.1890/03-0245

Jochum, K. P., Nohl, U., Herwig, K., Lammel, E., Stoll, B., & Hofmann, A. W. (2005). GeoReM: A new geochemical database for reference materials and isotopic standards. *Geostandards and Geoanalytical Research*, *29*(3), 333–338. https://doi.org/10.1111/j.1751-908X.2005.tb00904.x

Johnson, D W, & Henderson, G. S. (1989). Terrestrial nutrient cycling. In Johnson, D. W. & Van Hook, R. I. (Eds.), *Analysis of biogeochemical cycling processes in Walker branch watershed* (pp. 233–300). New York, NY: Springer New York. https://doi.org/10.1007/978-1-4612-3512-5_7

Kabata-Pendias, A. (2011). *Trace elements in soils and plants*. Boca Raton, FL; London, UK; and New York: CRC Press. https://doi.org/10.1201/b10158-25

Kennedy, M. J., Hedin, L. O., & Derry, L. A. (2002). Decoupling of unpolluted temperate forests from rock nutrient sources revealed by natural $^{87}Sr/^{86}Sr$ and ^{84}Sr tracer addition. *Proceedings of the National Academy of Sciences*, *99*(15), 9639–9644. https://doi.org/10.1073/pnas.152045499

Kleber, A., & Terhorst, B. (2013). Mid-latitude slope deposits (cover beds). In *Developments in sedimentology* (Vol. 66, pp. 1–302). Amsterdam, The Netherlands: Elsevier. https://doi.org/10.1016/B978-0-444-53118-6.09992-X

Lambers, H., Brundrett, M. C., Raven, J. A., & Hopper, S. D. (2011). Plant mineral nutrition in ancient landscapes: High plant species diversity on infertile soils is linked to functional diversity for nutritional strategies. *Plant and Soil*, *348*(1–2), 7–27. https://doi.org/10.1007/s11104-011-0977-6

Lambers, H., Shane, M. W., Cramer, M. D., Pearse, S. J., & Veneklaas, E. J. (2006). Root structure and functioning for efficient acquisition of phosphorus: Matching morphological and physiological traits. *Annals of Botany*, *98*(4), 693–713. https://doi.org/10.1093/aob/mcl114

Lang, F., Bauhus, J., Frossard, E., George, E., Kaiser, K., Kaupenjohann, M., et al. (2016). Phosphorus in forest ecosystems: New insights from an ecosystem nutrition perspective. *Journal of Plant Nutrition and Soil Science*, *179*, 129–135. https://doi.org/10.1002/jpln.201500541

Lang, F., Krüger, J., Amelung, W., Willbold, S., Frossard, E., Bünemann, E. K., et al. (2017). Soil phosphorus supply controls P nutrition strategies of beech forest ecosystems in Central Europe. *Biogeochemistry*, *136*(1), 5–29. https://doi.org/10.1007/s10533-017-0375-0

Larsen, I. J., Montgomery, D. R., & Greenberg, H. M. (2014). The contribution of mountains to global denudation. *Geology*, *42*(6), 527–530. https://doi.org/10.1130/G35136.1

Larsen, M. C. (2012). Landslides and sediment budgets in four watersheds in eastern Puerto Rico. In S. F. Murphy & R. F. Stallard (Eds.), *Water quality and landscape processes of four watersheds in eastern Puerto Rico*, *U.S. Geological Survey Professional Paper 1789* (pp. 153–178). U.S. Geological Survey.

Lauer, F., Pätzold, S., Gerlach, R., Protze, J., Willbold, S., & Amelung, W. (2013). Phosphorus status in archaeological arable topsoil relicts—Is it possible to reconstruct conditions for prehistoric agriculture in Germany? *Geoderma*, *207-208*(1), 111–120. https://doi.org/10.1016/j.geoderma.2013.05.005

Lawrence, C. R., & Neff, J. C. (2009). The contemporary physical and chemical flux of aeolian dust: A synthesis of direct measurements of dust deposition. *Chemical Geology*, *267*(1–2), 46–63. https://doi.org/10.1016/j.chemgeo.2009.02.005

Lequy, É., Conil, S., & Turpault, M. P. (2012). Impacts of aeolian dust deposition on European forest sustainability: A review. *Forest Ecology and Management*, *267*, 240–252. https://doi.org/10.1016/j.foreco.2011.12.005

Likens, G. E., Bormann, F. H., Pierce, R. S., Eaton, J. S., & Johnson, N. M. (1977). *Biogeochemistry of a forested ecosystem*. New York: Springer. https://doi.org/10.1007/978-1-4615-9993-7

Maathuis, F. J. (2009). Physiological functions of mineral macronutrients. *Current Opinion in Plant Biology*, *12*(3), 250–258. https://doi.org/10.1016/j.pbi.2009.04.003

Maher, K., & von Blanckenburg, F. (2016). Surface ages and weathering rates from ^{10}Be (meteoric) and ^{10}Be/^{9}Be: Insights from differential mass balance and reactive transport modeling. *Chemical Geology*, *446*, 70–86. https://doi.org/10.1016/j.chemgeo.2016.07.016

Mahowald, N., Jickells, T. D., Baker, A. R., Artaxo, P., Benitez-Nelson, C. R., Bergametti, G., et al. (2008). Global distribution of atmospheric phosphorus sources, concentrations and deposition rates, and anthropogenic impacts. *Global Biogeochemical Cycles*, *22*, GB4026. https://doi.org/10.1029/2008GB003240

McCulley, R. L., Jobbágy, E. G., Pockman, W. T., & Jackson, R. B. (2004). Nutrient uptake as a contributing explanation for deep rooting in arid and semi-arid ecosystems. *Oecologia*, *141*(4), 620–628. https://doi.org/10.1007/s00442-004-1687-z

McKean, J. A., Dietrich, W. E., Finkel, R. C., Southon, J. R., & Caffee, M. W. (1993). Quantification of soil production and downslope creep rates from cosmogenic ^{10}Be accumulations on a hillslope profile. *Geology*, *21*(4), 343–346. https://doi.org/10.1130/0091-7613(1993)021<0343:QOSPAD>2.3.CO;2

Meek, K., Derry, L., Sparks, J., & Cathles, L. (2016). ^{87}Sr/^{86}Sr, Ca/Sr, and Ge/Si ratios as tracers of solute sources and biogeochemical cycling at a temperate forested shale catchment, central Pennsylvania, USA. *Chemical Geology*, *445*, 84–102. https://doi.org/10.1016/j.chemgeo.2016.04.026

Meyer, J., & Likens, G. E. (1979). Transport and transformation of phosphorus in a forest stream ecosystem. *Ecology*, *60*(6), 1255–1269. https://doi.org/10.2307/1936971

Miller, E. K., Blum, J. D., & Friedland, A. J. (1993). Determination of soil exchangeable-cation loss and weathering rates using Sr isotopes. *Nature*, *362*(6419), 438–441. https://doi.org/10.1038/362438a0

Missong, A., Bol, R., Willbold, S., Siemens, J., & Klumpp, E. (2016). Phosphorus forms in forest soil colloids as revealed by liquid-state ^{31}P-NMR. *Journal of Plant Nutrition and Soil Science*, *179*, 159–167. https://doi.org/10.1002/jpln.201500119

Morselli, L., Bernardi, E., Vassura, I., Passarini, F., & Tesini, E. (2008). Chemical composition of wet and dry atmospheric depositions in an urban environment: Local, regional and long-range influences. *Journal of Atmospheric Chemistry*, *59*(3), 151–170. https://doi.org/10.1007/s10874-008-9099-9

Murphy, J., & Riley, J. (1962). A modified single solution method for the determination of phosphate in natural water. *Analytical Chemistry Acta*, *27*, 31–36. https://doi.org/10.1016/S0003-2670(00)88444-5

Navrátil, T. (2000). Beryllium in waters of Czech forested ecosystems and the release of Beryllium from granites. *GeoLines*, *12*, 18–40.

Nepstad, D. C., de Carvalho, C. R., Davidson, E. A., Jipp, P. H., Lefebvre, P. A., Negreiros, G. H., et al. (1994). The role of deep roots in the hydrological and carbon cycles of Amazonian forests and pastures. *Nature*, *372*(6507), 666–669. https://doi.org/10.1038/372666a0

Newman, E. (1995). Phosphorus inputs to terrestrial ecosystems. *Journal of Ecology*, *83*(4), 713–726. https://doi.org/10.2307/2261638

Pett-Ridge, J. C., Derry, L. A., & Barrows, J. K. (2009). Ca/Sr and ^{87}Sr/^{86}Sr ratios as tracers of Ca and Sr cycling in the Rio Icacos watershed, Luquillo Mountains, Puerto Rico. *Chemical Geology*, *267*(1–2), 32–45. https://doi.org/10.1016/j.chemgeo.2008.11.022

Pett-Ridge, J. C., Derry, L. A., & Kurtz, A. C. (2009). Sr isotopes as a tracer of weathering processes and dust inputs in a tropical granitoid watershed, Luquillo Mountains, Puerto Rico. *Geochimica et Cosmochimica Acta*, *73*(1), 25–43. https://doi.org/10.1016/j.gca.2008.09.032

Porder, S., & Ramachandran, S. (2013). The phosphorus concentration of common rocks—A potential driver of ecosystem P status. *Plant and Soil*, *367*(1–2), 41–55. https://doi.org/10.1007/s11104-012-1490-2

Porder, S., Vitousek, P. M., Chadwick, O. A., Chamberlain, C. P., & Hilley, G. E. (2007). Uplift, erosion, and phosphorus limitation in terrestrial ecosystems. *Ecosystems*, *10*(1), 159–171. https://doi.org/10.1007/s10021-006-9011-x

Poszwa, A., Dambrine, E., Ferry, B., Pollier, B., & Loubet, M. (2002). Do deep tree roots provide nutrients to the tropical rainforest? *Biogeochemistry*, *60*(1), 97–118. https://doi.org/10.1023/A:1016548113624

Poszwa, A., Dambrine, E., Pollier, B., & Atteia, O. (2000). A comparison between Ca and Sr cycling in forest ecosystems. *Plant and Soil*, *225*(1/2), 299–310. https://doi.org/10.1023/A:1026570812307

Poszwa, A., Ferry, B., Dambrine, E., Pollier, B., Wickman, T., Loubet, M., & Bishop, K. (2004). Variations of bioavailable Sr concentration and ^{87}Sr/^{86}Sr ratio in boreal forest ecosystems. *Biogeochemistry*, *67*(1), 1–20. https://doi.org/10.1023/B:BIOG.0000015162.12857.3e

Poszwa, A., Ferry, B., Pollie, B., Grimaldi, C., Charles-Dominique, P., Loubet, M., & Dambrine, E. (2009). Variations of plant and soil ^{87}Sr/^{86}Sr along the slope of a tropical inselberg. *Annals of Forest Science*, *66*(5), 512–513. https://doi.org/10.1051/forest/2009036

Poszwa, A., Wickman, T., Dambrine, E., Ferry, B., Dupouey, J. L., Helle, G., et al. (2003). A retrospective isotopic study of spruce decline in the Vosges mountains (France). *Water, Air, and Soil Pollution: Focus*, *3*(1), 201–222. https://doi.org/10.1023/A:1022176025379

Querejeta, J. I., Egerton-Warburton, L. M., & Allen, M. F. (2007). Hydraulic lift may buffer rhizosphere hyphae against the negative effects of severe soil drying in a California Oak savanna. *Soil Biology and Biochemistry*, *39*(2), 409–417. https://doi.org/10.1016/j.soilbio.2006.08.008

Richter, D. D., & Markewitz, D. (1995). How deep is soil? *BioSciece*, *45*(9), 600–609. https://doi.org/10.2307/1312764

Riotte, J., Maréchal, J. C., Audry, S., Kumar, C., Bedimo Bedimo, J. P., Ruiz, L., et al. (2014). Vegetation impact on stream chemical fluxes: Mule Hole watershed (South India). *Geochimica et Cosmochimica Acta*, *145*, 116–138. https://doi.org/10.1016/j.gca.2014.09.015

Rodionov, A., Bauke, S. L., von Sperber, C. Hoeschen, C., Kandeler, E., Kruse, J., et al. (2020). Biogeochemical cycling of phosphorus in subsoils of temperate forest ecosystems. *Biogeochemistry*. In press.

Santana, M. C., Pereira, A. P. A., Forti, V. A., & Cardoso, E. J. B. N. (2016). Eucalypt as trap plant to capture associative fungi in soil samples from great depth. *International Journal of Environmental & Agriculture Research (IJOEAR)*, *2*(5), 191–194.

Scatena, F. N., & Lugo, A. E. (1995). Geomorphology, disturbance, and the soil and vegetation of two subtropical wet steepland watersheds of Puerto Rico. *Geomorphology*, *13*(1–4), 199–213. https://doi.org/10.1016/0169-555X(95)00021-V

Schmid, I., & Kazda, M. (2002). Root distribution of Norway spruce in monospecific and mixed stands on different soils. *Forest Ecology and Management*, *159*(1–2), 37–47. https://doi.org/10.1016/S0378-1127(01)00708-3

Schmid, I., & Kazda, M. (2005). Clustered root distribution in mature stands of *Fagus sylvatica* and *Picea abies* Received. *Oecologia*, *144*, 25–35.

Schmitt, A. D., Gangloff, S., Labolle, F., Chabaux, F., & Stille, P. (2017). Calcium biogeochemical cycle at the beech tree-soil solution interface from the Strengbach CZO (NE France): Insights from stable Ca and radiogenic Sr isotopes. *Geochimica et Cosmochimica Acta*, *213*, 91–109. https://doi.org/10.1016/j.gca.2017.06.039

Schuessler, J. A., von Blanckenburg, F., Bouchez, J., Uhlig, D., & Hewawasam, T. (2018). Nutrient cycling in a tropical montane rainforest under a supply-limited weathering regime traced by elemental mass balances and Mg stable isotopes. *Chemical Geology*, *497*, 74–87. https://doi.org/10.1016/j.chemgeo.2018.08.024

Skřivan, P., Minařík, L., Burian, M., Martínek, J., Žigová, A., Dobešová, I., et al. (2000). Biogeochemistry of beryllium in an experimental forested landscape of the Lesni potok Catchment in Central Bohemia Czech Republic. *Geolines*, *12*, 41–62.

Stallard, R. F. (1995). Relating chemical and physical erosion. In A. F. White, & S. L. Brantley (Eds.), *Chemical weathering rates of silicate minerals: Reviews in mineralogy* (Vol. 31, pp. 543–564).

Stallard, R. F. (2012). Weathering, landscape equilibrium, and carbon in four watersheds in eastern Puerto Rico—Chapter H. In S. F. Murphy & R. F. Stallard (Eds.), *Water quality and landscape processes of four watersheds in eastern Puerto Rico*, *USGS Professional Paper 1789–H* (pp. 199–248). Reston, VA: U.S. Geological Survey. Retrieved from https://pubs.usgs.gov/pp/1789/pdfs/ChapterH.pdf

Taylor, S. R., & McLennan, S. M. (1995). The geochemical evolution of the continental crust. *Reviews of Geophysics*, *33*(2), 241–265. https://doi.org/10.1029/95RG00262

Tiessen, H., & Moir, J. (1993). Characterization of available P by sequential extraction. In M. R. Carter (Ed.), *Soil sampling and methods of analysis* (Vol. 7, pp. 75–86). Taylor & Francis Group. https://doi.org/10.1201/9781420005271.ch25

Tiessen, H. (2008). Phosphorus in the global environment. In P. J. White & J. P. Hammond (Eds.) *The ecophysiology of plant-phosphorus interactions* (Vol. 7, pp. 1–6). The Netherlands: Springer, Dordrecht. https://doi.org/10.1007/978-1-4020-8435-5_1

Turner, B. L., Lambers, H., Condron, L. M., Cramer, M. D., Leake, J. R., Richardson, A. E., & Smith, S. E. (2013). Soil microbial biomass and the fate of phosphorus during long-term ecosystem development. *Plant and Soil*, *367*(1–2), 225–234. https://doi.org/10.1007/s11104-012-1493-z

Uhlig, D., Schuessler, J. A., Bouchez, J., Dixon, J. L., & Von Blanckenburg, F. (2017). Quantifying nutrient uptake as driver of rock weathering in forest ecosystems by magnesium stable isotopes. *Biogeosciences*, *14*(12), 3111–3128. https://doi.org/10.5194/bg-14-3111-2017

Uhlig, D., & von Blanckenburg, F. (2019a). How slow rock weathering balances nutrient loss during fast forest floor turnover in montane, temperate Forest ecosystems. *Frontiers in Earth Science*, *7*(July), 1–28. https://doi.org/10.3389/feart.2019.00159

Uhlig, D., & von Blanckenburg, F. (2019b). Geochemical and isotope data on rock weathering, and nutrient balances during fast forest floor turnover in montane, temperate forest ecosystems. *GFZ Data Services*. https://doi.org/10.5880/GFZ.3.3.2019.004

Uhlig, D., Amelung, W., & von Blanckenburg, Friedhelm (2020). Chemical and isotope data on how mineral nutrients sourced in deep regolith sustain long-term nutrition of mountainous temperate forest ecosystems. *GFZ Data Services*. http://doi.org/10.5880/GFZ.3.3.2020.002

Uhlig, D., Goldberg, T., Frick, D. A., Blanckenburg, F. (2020). Quantifying beryllium concentrations in plant shoots from forest ecosystems using cation-exchange chromatography and quadrupole ICP-MS. *Analytical Science Advances*, *1*, 8–21. https://doi.org/10.1002/ansa.202000036

van der Heijden, G., Legout, A., Midwood, A. J., Craig, C. A., Pollier, B., Ranger, J., & Dambrine, E. (2013). Mg and Ca root uptake and vertical transfer in soils assessed by an in situ ecosystem-scale multi-isotopic (^{26}Mg & ^{44}Ca) tracing experiment in a beech stand (Breuil-Chenue, France). *Plant and Soil*, *369*(1–2), 33–45. https://doi.org/10.1007/s11104-012-1542-7

Vance, C. P., Uhde-Stone, C., & Allan, D. L. (2003). Phosphorus acquisition and use: Critical adaptations by plants for securing a nonrenewable resource. *New Phytologist*, *157*(3), 423–447. https://doi.org/10.1046/j.1469-8137.2003.00695.x

Vanderstraeten, P., Lénelle, Y., Meurrens, A., Carati, D., Brenig, L., Delcloo, A., et al. (2008). Dust storm originate from Sahara covering Western Europe: A case study. *Atmospheric Environment*, *42*(21), 5489–5493. https://doi.org/10.1016/j.atmosenv.2008.02.063

Vitousek, P. M., & Farrington, H. (1997). Nutrient limitation and soil development: Experimental test of a biogeochemical theory. *Biogeochemistry*, *37*(1), 63–75. https://doi.org/10.1023/A:1005757218475

von Blanckenburg, F., Belshaw, N. S., & O'Nions, R. K. (1996). Separation of ^{9}Be and cosmogenic ^{10}Be from environmental materials and SIMS isotope dilution analysis. *Chemical Geology*, *129*(1–2), 93–99. https://doi.org/10.1016/0009-2541(95)00157-3

von Blanckenburg, F., Bouchez, J., & Wittmann, H. (2012). Earth surface erosion and weathering from the ^{10}Be (meteoric)/^{9}Be ratio. *Earth and Planetary Science Letters*, *351–352*, 295–305. https://doi.org/10.1016/j.epsl.2012.07.022

von Blanckenburg, F., Hewawasam, T., & Kubik, P. W. (2004). Cosmogenic nuclide evidence for low weathering and denudation in the wet, tropical highlands of Sri Lanka. *Journal of Geophysical Research*, *109*, F03008. https://doi.org/10.1029/2003JF000049

von Blanckenburg, F., Wittmann, H., & Schuessler, J. A. (2016). HELGES: Helmholtz Laboratory for the geochemistry of the earth surface. *Journal of Large-Scale Research Facilities*, *2*, 1–5. https://doi.org/10.17815/jlsrf-2-141

Walker, T. W., & Syers, J. K. (1976). The fate of phosphorus during pedogenesis. *Geoderma*, *15*(1), 1–19. https://doi.org/10.1016/0016-7061(76)90066-5

Wardle, D. A., Walker, L. R., & Bardgett, R. D. (2004). Ecosystem properties and forest decline in constrasting long-term chronosequences. *Science*, *305*(5683), 509–513. https://doi.org/10.1126/science.1098778

Wilcke, W., Velescu, A., Leimer, S., Bigalke, M., Boy, J., & Valarezo, C. (2017). Biological versus geochemical control and environmental change drivers of the base metal budgets of a tropical montane forest in Ecuador during 15 years. *Biogeochemistry*, *136*(2), 167–189. https://doi.org/10.1007/s10533-017-0386-x

Wilcke, W., Yasin, S., Abramowski, U., Valarezo, C., & Zech, W. (2002). Nutrient storage and turnover in organic layers under tropical montane rain forest in Ecuador. *European Journal of Soil Science*, *53*(1), 15–27. https://doi.org/10.1046/j.1365-2389.2002.00411.x

Willenbring, J. K., & von Blanckenburg, F. (2010). Meteoric cosmogenic Beryllium-10 adsorbed to river sediment and soil: Applications for earth-surface dynamics. *Earth-Science Reviews*, *98*(1–2), 105–122. https://doi.org/10.1016/j.earscirev.2009.10.008

Wittmann, H., Von Blanckenburg, F., Bouchez, J., Dannhaus, N., Naumann, R., Christl, M., & Gaillardet, J. (2012). The dependence of meteoric ^{10}Be concentrations on particle size in Amazon River bed sediment and the extraction of reactive ^{10}Be/^{9}Be ratios. *Chemical Geology*, *318–319*, 126–138. https://doi.org/10.1016/j.chemgeo.2012.04.031

Wittmann, H., Von Blanckenburg, F., Dannhaus, N., Bouchez, J., Gaillardet, J., Guyot, J. L., et al. (2015). A test of the cosmogenic ^{10}Be(meteoric)/^{9}Be proxy for simultaneously determining basin-wide erosion rates, denudation rates, and the degree of weathering in the Amazon basin. *Journal of Geophysical Research: Earth Surface*, *120*, 2498–2528. https://doi.org/10.1002/2015JF003581

Zender, C. S., Bian, H., & Newman, D. (2003). Mineral dust entrainment and deposition (DEAD) model: Description and 1990s dust climatology. *Journal of Geophysical Research*, *108*(D14), 4416. https://doi.org/10.1029/2002JD002775